学 位 論 文

Infection dynamics of coronavirus disease 2019 (COVID-19)

(新型コロナウイルス感染症の感染動態に関する研究)

2022年 3月

北海道大学

Sung-mok Jung

（スンモク・ジョン）

学 位 論 文

Infection dynamics of coronavirus disease 2019 (COVID-19)

(新型コロナウイルス感染症の感染動態に関する研究)

2022年 3月

北海道大学

Sung-mok Jung

（スンモク・ジョン）

Table of contents

List of publications and presentations

Publications in this thesis:

1. Jung S-m, Akhmetzhanov AR, Hayashi K, Linton NM, Yang Y, Yuan B, Kobayashi T, Kinoshita R, Nishiura H. Real-time estimation of the risk of death from novel coronavirus (COVID-19) infection: inference using exported cases. *J Clin Med*. 2020;9(2)523.
2. Jung S-m, Endo A, Kinoshita R, Nishiura H. Projecting a second wave of COVID-19 in Japan with variable interventions in high-risk settings. *R. Soc. Open Sci*. 2021;8(3),202169.
3. Jung S-m, Endo A, Akhmetzhanov AR, Nishiura H. Predicting the effective reproduction number of COVID-19: inference using human mobility, temperature, and risk awareness. *Int J Infect Dis*. 2021;113:47-54.

Related publications:

4. Jung S-m, Kinoshita R, Thompson R, Linton NM, Yang Y, Akhmetzhanov AR, Nishiura H. Epidemiological identification of a novel pathogen in real time: Analysis of the atypical pneumonia outbreak in Wuhan, China, 2019–2020. *J Clin Med* 2020;9(3):637.
5. Nishiura H, Jung S-m, Linton NM, Kinoshita R, Yang Y, Hayashi K, Kobayashi T, Yuan B, Akhmetzhanov AR. The extent of transmission of Novel Coronavirus in Wuhan, China, 2020. *J Clin Med* 2020;9(2):330.
6. Nishiura H, Kobayashi T, Miyama T, Suzuki A, Jung S-m, Hayashi K, Kinoshita R, Yang Y, Yuan B, Akhmetzhanov AR, Linton NM. Estimation of the asymptomatic ratio of novel coronavirus infections (COVID-19). *Int J Infect Dis*. 2020;94:154–155.

Research presented in this thesis has been shared at conferences as listed below:

1. "The impact of human mobility pattern on the effective reproduction number of COVID-19 in Japan." The 91st Annual Meeting of the Japan Society for Hygiene. March 6–8, 2021. Oral presentation. Online. Domestic conference.

Summary

Background and Objectives: The first confirmed case of severe acute respiratory syndrome coronavirus 2 (SARS-CoV-2) infection was reported in January 2020, and the transmission of its causative agent, coronavirus disease 2019 (COVID-19) has rapidly spread around the world. In the early phase of the epidemic, knowledge of the confirmed case fatality risk (cCFR) and basic reproduction number (R_0) are crucial to characterize the severity and determine the pandemic potential of an emerging infectious disease. Thus, in order to assess the risk of COVID-19, *Chapter 1* statistically estimated these two epidemiological measurements of COVID-19, using the exported cases which allow for an estimate of the cumulative number of SARS-CoV-2 infections in mainland China. In addition, *Chapter 2* explored prospective exit strategies by projecting a second wave of the COVID-19 epidemic in Japan with different levels of restriction to suggest a more sustainable strategy than the current restrictive guideline. Lastly, the effective reproduction number (R_t) has been used as an essential indicator for assessing the effectiveness of countermeasures during the COVID-19 pandemic. However, conventional methods relying on the reported case counts are unable to provide timely R_t due to the time delay from infection to report. *Chapter 3* suggested a simple statistical framework for predicting R_t in near real-time, using timely accessible data of possible driving factors of SARS-CoV-2 transmissions (i.e., human mobility, temperature, and risk awareness).

Chapter 1: Real-time estimation of the risk of death from COVID-19: inference using exported cases

Methods: Using the exponential growth rate of the estimated cumulative incidence from exportation cases and accounting for the time delay from illness onset to death, the cCFR and R_0 were estimated. We modelled epidemic growth either from a single reported index case with illness onset on 8 December 2019 (Scenario 1) and using the growth rate fitted along with the other parameters (Scenario 2) based on 20 exported cases reported by 24 January 2020. **Results:** The cumulative incidence in China by 24 January was estimated at 6,924 cases (95% confidence interval [CI]: 4,885–9,211) and 19,289 cases (95% CI: 10,901–30,158), respectively. The latest estimated values of the cCFR were 5.3% (95% CI: 3.5%–7.5%) for Scenario 1 and 8.4% (95% CI: 5.3%–12.3%) for Scenario 2. The R_0 was estimated to be 2.1 (95% CI: 2.0–2.2) and 3.2

(95% CI: 2.7–3.7) for Scenarios 1 and 2, respectively. **Discussion:** Based on these estimates, we argued that the current COVID-19 epidemic has a substantial potential for causing a pandemic. The proposed approach provides insights into early risk assessment using publicly available data.

Chapter 2: Projecting a second wave of COVID-19 in Japan with variable interventions in high-risk settings

Methods: We quantified the next-generation matrix, accounting for high- and low-risk settings of SARS-CoV-2 transmissions. Then, the matrix was used to project the future incidence in Tokyo and Osaka after the first state of emergency is lifted, presenting multiple post-emergency scenarios with different levels of restriction. **Results:** The R_t for the increasing phase, the transition phase and the state-of-emergency phase in the first wave of the disease were estimated as 1.78 (95% credible interval (CrI): 1.73–1.82), 0.74 (95% CrI: 0.71–0.78) and 0.63 (95% CrI: 0.61–0.65), respectively, in Tokyo and as 1.58 (95% CrI: 1.51–1.64), 1.20 (95% CrI: 1.15–1.25) and 0.48 (95% CrI: 0.44–0.51), respectively, in Osaka. Projections showed that a 50% decrease in the high-risk transmission is required to keep R_t less than 1 in both locations—a level necessary to maintain control of the epidemic and minimize the burden of disease. **Discussion:** Compared with stringent interventions such as lockdowns, our proposed exit strategy from restrictive guidelines, focusing intervention efforts on the high-risk setting, allows socioeconomic activities to be maintained while minimizing the risk of a resurgence of the disease.

Chapter 3: Predicting the effective reproduction number of COVID-19: inference using human mobility, temperature, and risk awareness.

Methods: A linear regression model to predict R_t was designed and embedded in the renewal process. Four prefectures of Japan with high incidences in the first wave were selected for model fitting and validation. Predictive performance was assessed by comparing the observed and predicted incidences using cross-validation, and by testing on a separate dataset in two other prefectures with distinct geographical and climatological settings from the four studied prefectures. **Results:** The predicted mean values of R_t and 95% uncertainty intervals followed the overall trends for incidence, while predictive performance was partially diminished when R_t changed abruptly, potentially due to superspreading events or when stringent countermeasures were implemented. In addition, the predictive performance of the best-ranked model on the

separate test data indicates the applicability of the proposed model to other geographical settings. **Discussion:** The described model can potentially be used for monitoring the transmission dynamics of COVID-19 ahead of the formal estimates, subject to time delay, providing essential information for timely planning and assessment of countermeasures.

Conclusion: Since the SARS-CoV-2 emerged, it has posed an enormous threat to healthcare systems all around the world. The present dissertation has contributed to a better knowledge of COVID-19 infection dynamics, which is crucial for controlling the ongoing COVID-19 pandemic and devising timely and proper COVID-19 response strategies. First, it estimated the risk of death and transmissibility of COVID-19 for the early risk assessment. In addition, it projected the future dynamics of COVID-19 by reconstructing the next-generation matrix accounting for high- and low-risk transmission settings, and quantitatively assessed the impacts of possible exit strategies on the SARS-CoV-2 transmissions in Japan. Lastly, it suggested the statistical framework for providing timely prediction of the effective reproduction number, that can be used before a formal estimate is available. Despite uncertainties surrounding new SARS-CoV-2 variants, these series of studies can shed light on a better understanding of the infection dynamics of COVID-19 and the establishment of evidence-based response strategies for minimizing the burden of the ongoing COVID-19 pandemic.

List of abbreviations

CFR	Case fatality risk
cCFR	Confirmed case fatality risk
CI/CrI	Confidence/credible interval
COVID-19	Coronavirus disease 2019
IFR	Infection fatality risk
Google mobility	Google community mobility reports
MCMC	Markov chain Monte Carlo
MERS	Middle East respiratory syndrome
R_0	Basic reproduction number
R_t	Effective reproduction number
RMSE	Root mean square errors
SARS	Severe acute respiratory syndrome
SARS-CoV-2	Severe acute respiratory syndrome coronavirus 2
SD	Standard deviation
WHO	World Health Organization

Introduction

In early December 2019, a cluster of pneumonia cases of unknown etiology has emerged in Wuhan, China. A rapid virological investigation identified the causative pathogen as a severe acute respiratory syndrome coronavirus 2 (SARS-CoV-2) and the disease was named coronavirus disease 2019 (COVID-19). Originally the main mode of SARS-COV-2 transmissions was considered as a common-source zoonotic exposure in a local wet market in Wuhan (Chinese National Health Commission (NHC), 2021). However, even after shutting down the market, sustained transmissions were reported across China, and the human-to-human transmission was found later to be common (Jung et al., 2020a).

As the COVID-19 was rapidly spread to other countries through international travelers, a risk assessment of the severity of infection and transmissibility was highly required to quantify the pandemic potential of the COVID-19 and anticipate the likely impact on healthcare settings by the end of the epidemic. Despite early risk assessment of a newly emerged disease is challenging due to the underestimation in the reported case counts, the exported cases that were confirmed outside China could provide an avenue to inferring the actual cumulative case counts in China (Nishiura et al., 2020a). Thus, *Chapter 1* presented early estimates of the confirmed case fatality risk (cCFR) and basic reproduction number (R_0) —the average number of secondary cases generated by a single primary case in a naïve population—of COVID-19, using the growth rate of the estimated cumulative incidence from exportation cases and accounting for the time delay from illness onset to death.

With the rapid spread of COVID-19, a various set of non-pharmaceutical interventions (NPIs), including the closure of bars and restaurants and voluntary limitation of non-household contact, was implemented in many of the heavily affected areas (Perra, 2021). As the upsurge of COVID-19 incidence was observed in April 2020, the Japanese national government also declared the first state of emergency and such stringent interventions greatly contributed to suppressing the disease incidence of COVID-19 in Japan (Ministry of Health Labour and Welfare, 2020a). However, given its considerable socioeconomic impacts, these restrictions must eventually be replaced by a more sustainable strategy. To characterize such an exit strategy from the restrictive guidelines, *Chapter 2* quantified the next-generation matrix accounting for high- and low-risk

settings. Then, based on the reconstructed next-generation matrix, future waves of SARS-CoV-2 infections with different levels of restriction were projected to provide an evidence-based guideline for sustainable response strategy that allows society to be resumed while minimizing the risk of a resurgence of the disease.

As the pandemic continuous, monitoring of the effective reproduction number (R_t) —the expected number of secondary cases arising from a single primary case at calendar time t—has played an essential role in understanding the infection dynamics and evaluating the countermeasures (Nishiura and Chowell, 2009; Thompson et al., 2019a). However, due to the time delay from infection to reporting, conventional methods relying on the reported case counts are unable to provide timely R_t (Gostic et al., 2020). Accumulated evidence suggests that integrating human mobility with temperature and risk awareness reflects contact patterns as a function of time (Leung et al., 2021; Smith et al., 2021; West et al., 2020), and these data are more readily accessible than case counts. Therefore, *Chapter 3* suggested a statistical framework to provide the proxy of R_t in a near real-time manner, using the possible driving factors of COVID-19 transmissions. All three chapters of the present dissertation explored the infection dynamics of COVID-19 and provided an opportunity for developing proper and timely control measures in the corresponding periods of the COVID-19 pandemic.

Chapter 1: Real-time estimation of the risk of death from COVID-19: inference using exported cases

Background

In early December 2019, clusters of pneumonia cases of unknown etiology were reported in Wuhan, China (Jung et al., 2020b; Li et al., 2020b; The World Health Organization, 2020a). As extensive transmissions were observed, the World Health Organization (WHO) carried out an active virological investigation, and the causative agent was identified as "severe acute syndrome coronavirus 2" (Cui et al., 2019). The virus rapidly spread to other regions in China, resulting in a total of 4,515 cases including 106 deaths as of 27 January 2020 (Center for Disease Control and Prevention, 2020). In addition, 41 cases of SARS-CoV-2 infections were confirmed in other parts of the world, including other Asian countries, the United States, France, Australia, and Canada, indicating its considerable transmissibility. In response, the Chinese government imposed a lockdown on the city of Wuhan on 23 January 2020, shutting down inbound and outbound travels across the affected areas, along with placing all corresponding residents under stringent home quarantine (Lau et al., 2020).

Since many of the cases in the initial cluster were associated with a local wet market—a place that sells seafood and wild animals—in Wuhan, a common-source zoonotic exposure was suspected as the main route of the transmissions (Huang et al., 2020). However, even after shutting down the market, sustained transmissions of SARS-CoV-2 were continuously observed across China, along with several household transmissions (Chan et al., 2020). Such evidence implies that human-to-human transmission has aided in the establishment of the rapid emergence of incidence (The World Health Organization, 2020b), and accordingly the reported case counts might greatly underestimate the actual number of infections in mainland China (Nishiura et al., 2020a).

With the accumulative evidence of human-to-human transmissions, the early risk assessment has become more essential to guide the extent and direction of control measures in the early stage of the epidemic. As seen in the severe acute respiratory syndrome (SARS) outbreak in 2003, developing timely response strategies based on those epidemiological indicators can

significantly reduce the ultimate burden of the disease (Kobayashi et al., 2020). Therefore, the early assessment of the severity of infection and transmissibility of COVID-19 is highly required, which can reveal important information about the likely number of deaths by the end of the epidemic and the pandemic potential of the disease.

One important epidemiological indicator of the severity of the disease is case fatality risk (CFR), which can be measured by the following three approaches: (i) the proportion of the cumulative number of deaths out of the cumulative number of cases at a point in time, (ii) the ratio of the cumulative number of deaths to the cumulative number of infected individuals whose clinical outcome is known (i.e., the deceased or recovered), and (iii) the risk of death among confirmed cases (referred to as "cCFR" (Nishiura et al., 2009)) with an explicit consideration of the time delay from illness onset to death (Ghani et al., 2005). Estimating the CFR relied on the method (iii) (i.e., estimation of cCFR) can provide less biased insight into the severity of the disease, especially in a real-time manner, because the naïve CFR based on method (i) tends to be an underestimate due to the growth of fatal cases. For instance, right-censored cases with respect to time delay from illness onset to death may lead to underestimation of the CFR, since deaths related to the infection may yet occur after case identification (Garske et al., 2009; Ghani et al., 2005; Nishiura et al., 2009). However, with a certain level of underascertainment bias in the number of cases, the cCFR may overestimate the actual CFR among all infected individuals (referred to as "IFR"). If patients with mild symptoms or undistinguished clinical signs (compared to other respiratory infections) are not fully recognized as suspected cases, the denominator of cCFR (i.e., confirmed cases) may include only part of actual infections unless active molecular diagnostic testing or seroprevalence survey is performed together. Nonetheless, the cCFR is still a valuable epidemiological measure showing the upper bound of the CFR among all symptomatic cases, particularly in circumstances with a high uncertainty such as the emergence of a new human pathogen like COVID-19.

Moreover, estimating the basic reproduction number (R_0) —the average number of secondary cases generated by a single primary case in a fully susceptible population—can reveal the pandemic potential of the disease, given the definition of a pandemic as the worldwide spread of a newly emerged disease (Thompson et al., 2019b). Therefore, the present study aims to estimate

the cCFR and R_0 of the COVID-19 in a real-time manner, using the growth rate of the estimated cumulative incidence in China from exportation cases and accounting for the empirically observed time delay from illness onset to death.

Methods

Epidemiological data

Information on (i) exported COVID-19 cases confirmed outside China and (ii) COVID-19 related deaths in China were retrieved from the first announcement date of the current outbreak (i.e., 31 December 2019) through 24 January 2020. The latter timeframe was determined to consider the impact of the ban on public transportation from Wuhan (including flights) which was imposed by the Chinese government on 23 January 2020 on the number of exported cases (BBC NEWS). All data were collected either from government websites or from media quoting government announcements. In detail, our data includes 51 exported COVID-19 cases and 41 deaths related to the disease in China.

Estimation of the Delay Distributions

The number of newly infected cases by date of illness onset *t*, *i*(*t*), is modelled using an exponential growth model with the rate *r*: $i(t) = i_0 e^{rt}$, where i_0 indicated the expected number of infected cases at time $t = 0$. The cumulative incidence, *I*(t), is an integral of *i*(*t*) over the time interval from 0 to *t* that can be written as $I(t) = \int_0^t i(s)\mathrm{d}s = i_0(e^{rt} - 1)/r$. The cumulative incidence is adjusted to the date of report by the factor *u* dependent on the parameters of the delay distribution. For the estimation of time delay distribution from illness onset to death, we borrowed parameters from an earlier study that accounted for the right-truncation (Linton et al., 2020). Let $f(t;\theta)$ be the lognormal distribution with parameters $\theta_d = \{a_d, b_d\}$. Then, the cumulative incidence *I(t)* by date of report *t* can be adjusted to the time from illness onset to death and report by simply multiplying it by the factor $u(r, \theta_d)$, which is a consequence of the exponentially growing epidemic (Nishiura et al., 2009). The factor *u* is defined by the following integral*:*

$$u(r,\theta_d) = \int_0^\infty \exp(-rs)\, f(s;\theta_d) ds \qquad (1)$$

The adjusted cumulative incidence then obeys $u(r,\theta_d) \cdot I(t)$. The cumulative number of deaths $D(t)$ reported by date t is the result of binomial sampling:

$$D(t) \sim \text{binom}(\text{size} = u(r,\theta_d) \cdot I(t), \text{prob} = CFR(t)) \qquad (2)$$

Let a_e and b_e be the shape and inverse scale of the gamma distribution modeling the distribution of time interval from illness onset to the report for observed exported cases. The cumulative incidence in China can be then adjusted by the multiplicative factor $\tilde{u}(r,\theta_e = \{a_e, b_e\})$. The number of exported cases $E(t)$ can then be sampled from another Binomial distribution:

$$E(t) \sim \text{binom}(\text{size} = \tilde{u}(r,\theta_e) \cdot I(t), \text{prob} = p) \qquad (3)$$

where p describes the probability of finding a traveler from Wuhan among all travelers from China subject to the detection time window of the virus T = 12.5 days (Nishiura et al., 2020a). Given that the total volume of inbound passengers from China is M = 5.56 million passengers per year, the fraction of Wuhan travelers is ϕ = 0.021%, and the population of Wuhan is n = 11 million, the probability p is given by

$$p = \frac{\phi M T}{365 n} \approx 0.0036 \qquad (4)$$

Statistical model

First, we fitted the delay distribution of the time from illness onset to report $\Delta T_{e,k}$ $(k \le K_e)$ to the gamma distribution. We define the log-likelihood as follows:

$$logL_e(\theta_e | \Delta T_{e,k}) = \sum_k \log(\text{gamma}(\Delta T_{e,k} \mid \text{shape} = a_e, \text{scale} = b_e) \qquad (5)$$

and it was maximized to estimate the parameters $\tilde{\theta}_e = \{\tilde{a}_e, \tilde{b}_e\}$, used in the following step.

Second, we fitted the observed counts of exported cases and deaths by considering two other likelihoods respective to each process:

$$logL_E(\{r, i_0\} \mid \{E(t), t_e \le t \le T\}) = \sum_{t=t_e}^{T} \log\Big(\text{binom}\big(E(t) \mid \text{size} = \tilde{u}(r, \tilde{\theta}_e) \cdot I(t), \text{prob} = p\big)\Big) \quad (6)$$

$$logL_E(\{r, i_0\} \mid \{E(t), t_e \le t \le T\}) = \sum_{t=t_e}^{T} \log\Big(\text{binom}\big(E(t) \mid \text{size} = \tilde{u}(r, \tilde{\theta}_e) \cdot I(t), \text{prob} = p\big)\Big) \quad (7)$$

where t_e and t_d are the times at which the first exportation event and the first death are observed. The total log-likelihood is given by the sum of two log-likelihoods:

$$logL_\Sigma\big(\theta_\Sigma = \{r, i_0, \text{CFR}(t)\} | D(t), E(t)\big) = logL_E\big(\{r, i_0\} | E(t)\big) + logL_D\big(\{r, i_0, CFR(t)\} | D(t)\big) \quad (8)$$

which is then maximized to determine the best-fit parameters $\{r, i_0, CFR(t)\}$.

We considered two possible scenarios to fit to the data. In the first scenario (referred to as "Scenario 1"), we fixed the parameter i_0 as one on the date of illness onset for the first COVID-19 confirmed case (i.e., 8 December 2019; assuming that the first confirmed case as a real initial case), providing a fixed starting point for the exponential growth of the cumulative incidence. Since there is still uncertainty using this date as a proxy for the beginning of exponential growth due to inconsistencies in reported illness onset for the earliest reported cases (Huang et al., 2020; Li et al., 2020b), we conducted a sensitivity analysis where the start date for exponential growth was varied between 1 December and 10 December 2019. In the second scenario (referred to as "Scenario 2"), all parameters $\{r, i_0, CFR(t)\}$ are variable, and the calculation begins on the date the first exported case was observed (i.e., 13 January 2020). For both scenarios, we validated sensitivities in the estimated growth rate, cumulative incidence, and cCFR value related to different cut-off times, values of the detection window *T*, and sizes of the catchment population of the Wuhan International airport *n*.

The basic reproduction number R_0 for the COVID-19 epidemic was calculated as

$$R_0 = 1 + rS \quad (9)$$

where r is the estimated growth rate for each scenario and S is the mean serial interval. The value of the serial interval was adopted from a published study (Li et al., 2020b) in which the gamma distribution was fitted to six infector-infectee pairs (mean = 7.5 days, standard deviation [SD] = 3.4 days).

In our analysis, we employed Markov chain Monte Carlo (MCMC) simulations with eight chains of 4,250 samples each, with 2,500 samples used for the tuning stage, leveraging the No-U-Turn sampler (NUTS) part of the Python PyMC3 package. However, one of the input variables for the Binomial distribution $\tilde{u}(r, \theta_e) \cdot I(t)$ or $u(r, \theta_d) \cdot I(t)$ was modelled with a continuous variable in our approach. We used the gamma distribution, matching the first two moments to obtain the transformation of the discrete Binomial distribution to its continuous approximation (Li et al., 2018; Lipsitch et al., 2003). We avoided joint estimation of all parameters $\{\theta_\Sigma, \theta_e, \theta_d\}$ due to heterogeneity in the aggregated data—a similar issue is discussed in the previous study (Nishiura et al., 2009). Instead, we implemented sequential fitting, wherein first we considered only the likelihood L_e, then we fit the likelihood L_Σ using the mean values of the estimated parameters obtained in the previous round. Finally, we verified the obtained fit by calculating pointwise estimates using maximum likelihood estimation with confidence intervals derived as profile likelihood-based intervals. We found that both approaches were in complete agreement in their results.

Results

Figure 1 shows the mean and SD of the time delay from illness onset to reporting (Figure 1A) and death (Figure 1B). The mean time delay from illness onset to reporting among exported cases was estimated as 7.1 days (95% confidence interval [CI]: 5.9–8.4), while the time delay from illness onset to death was 20.2 days (95% CI: 15.1–29.5) (Linton et al., 2020).

The estimated cumulative incidence of COVID-19 in China using the exported case data and fitting an exponential growth curve for both Scenarios 1 and 2 were shown in Figure 2. As of 24 January, when 20 exported cases were reported, the cumulative incidence in China was estimated

as 6,924 cases (95% CI: 4,885–9,211) in Scenario 1 and 19,289 cases (95% CI: 10,901–30,158) in Scenario 2. The exponential growth rates (*r*), derived from the growth rate of cumulative incidence, were estimated as 0.15 per day (95% CI: 0.14–0.15) and 0.29 per day (95% CI: 0.22–0.36) in Scenarios 1 and 2, respectively. Table presents the real-time update of the estimated cumulative incidence in China by the date of reporting as the number of exported cases increases.

Figures 2C and 2D show the estimated cCFR value accounting for the time delay from illness onset to death under Scenarios 1 and 2, respectively. A total of 41 confirmed deaths were reported as of 24 January, the cCFR value was estimated at 5.3% (95% CI: 3.5–7.5%) for Scenario 1 and 8.4% (95% CI: 5.3–12.3%) for Scenario 2, respectively. Figure 3 shows the estimated R_0 for the COVID-19 infection, using the estimated exponential growth (*r*) and the possible range of the mean serial interval. Given that the serial interval is 7.5 days (Li et al., 2020b), the R_0 was estimated at 2.10 (95% CI: 2.04–2.16) and 3.19 (95% CI: 2.66–3.69) for Scenarios 1 and 2, respectively. As the mean serial interval varies, the estimates can range from 1.6 to 2.6 and 2.2 to 4.2 for Scenarios 1 and 2, respectively.

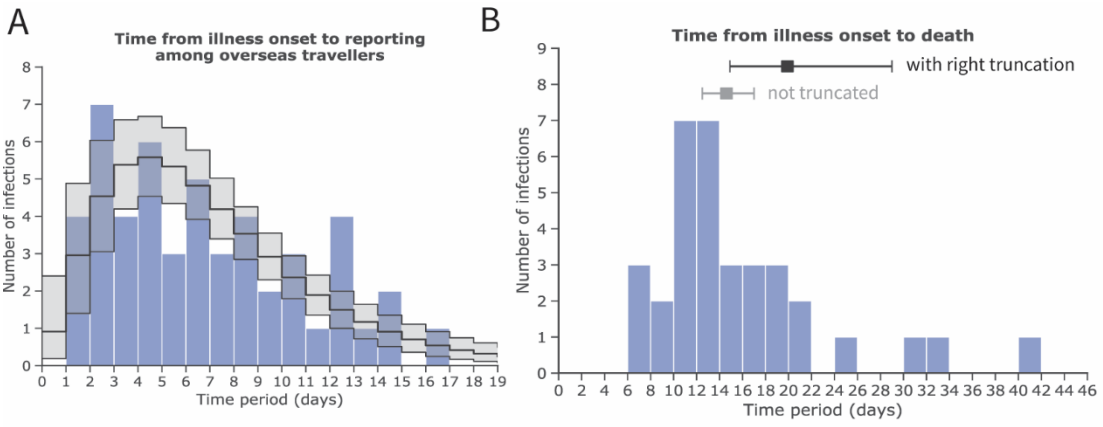

Figure 1. Estimates of the mean and standard deviation (SD) of the time from illness onset to reporting and death cases, accounting for right truncation, with novel coronavirus (COVID-19) infection in China, 2020

Inference of A and B was conducted among (A) exported cases observed in other countries and (B) deceased cases in China. (A) Frequency distribution of the time from illness onset to reporting among exported cases employing a gamma distribution with a mean of 7.1 days (95% confidence interval [CI]: 5.9–8.4) and SD of 4.4 days (95% CI: 3.5–5.7). (B) Frequency distribution of the time from illness onset to death with a mean of 19.9 days (95% CI: 14.9–29.0) (shown in black) and SD of 11.4 days (95% CI: 6.5–21.6) employing a lognormal distribution and accounting for right truncation. For reference, the estimate of the mean and its 95% credible intervals without accounting for right truncation are shown in grey. The values for the distribution of time from illness onset to death are borrowed from an earlier study (Linton et al., 2020). The blue bars show empirically observed data collected from governmental reports (as of 24 January 2020).

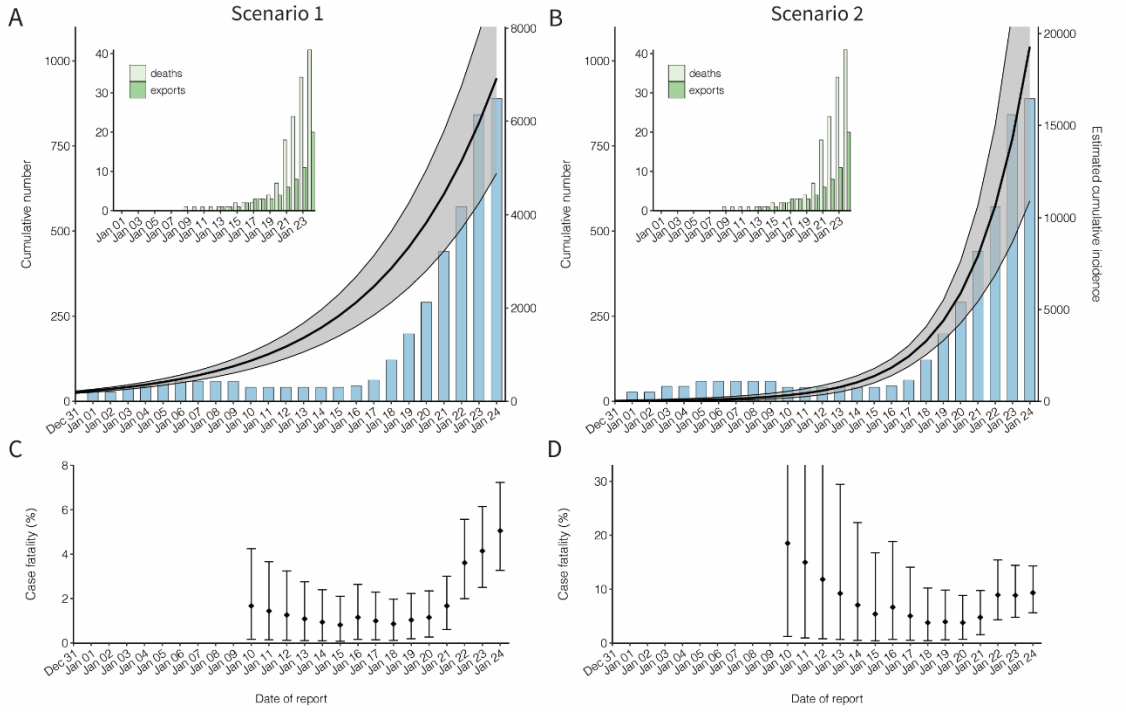

Figure 2. Cumulative incidence and the confirmed case fatality risk of the novel coronavirus (COVID-19) outbreak in China, 2020.

(A & B) Observed and estimated cumulative number of cases in China by the date of report. An exponential growth curve was extrapolated using the exported case data. Scenario 1 extrapolated the exponential growth from December to the first case on 8 December 2019, while Scenario 2 started the estimation of the exponential growth only from 13 January 2020. The black line and shaded area represent median and 95% credible interval of the cumulative incidence in China, respectively. The blue bars show the cumulative number of reported cases from the government of mainland China. The cumulative number of reported cases was not used for fitting, but it was shown for comparison between the cumulative number of reported and estimated cases in China. There is a decrease in the cumulative number of reported cases in early January, because only 41 cases tested positive for the novel coronavirus among the reported 59 cases on 10 January 2020. Left-top panels on both A and B show the cumulative numbers of exported cases observed in other countries and the cumulative number of deaths in China, represented by dark and light green bars, respectively. (C & D) Confirmed case fatality risk (cCFR) by the date of reporting. Each value of cCFR was estimated as the ratio of cumulative number of estimated incidences to death at time t. The points and error bars represent the median and its 95% credible interval of the cCFR. All 95% credible intervals were derived from Markov chain Monte Carlo simulations.

Table 1. Exportation events and estimated incidence in China, 2020

Importing Locations	Date of Report (2020)	Cumulative Count	Estimated Incidence in China (95% CI)	
			Scenario 1	Scenario 2
Thailand	13 January	1	1,828 (1,397–2,288)	1,369 (1,003–1,782)
Japan	16 January	2	2,120 (1,605–2,672)	1,829 (1,392–2,309)
Thailand	17 January	3	2,458 (1,845–3,119)	2,444 (1,894–3,033)
South Korea	20 January	4	3,832 (2,802–4,962)	5,882 (4,252–7,629)
Taiwan, United States	21 January	6	4,443 (3,220–5,792)	7,901 (5,425–10,662)
Thailand	22 January	8	5,151 (3,700–6,761)	10,626 (6,897–15,003)
Singapore, Vietnam	23 January	11	5,972 (4,252–7,892)	14,308 (8,661–21,250)
Japan, Nepal, South Korea, Singapore, Thailand, United States	24 January	20	6,924 (4,885–9,211)	19,289 (10,901–30,158)

CI: confidence interval (the 95% CI was derived from the Markov chain Monte Carlo method). Scenario 1 indicates the estimated exponential growth rate with the assumed illness onset date of the first COVID-19 case (i.e., 8 December 2019), while Scenario 2 presents the estimated exponential growth rate from the date of the first exportation event (i.e., 13 January 2020).

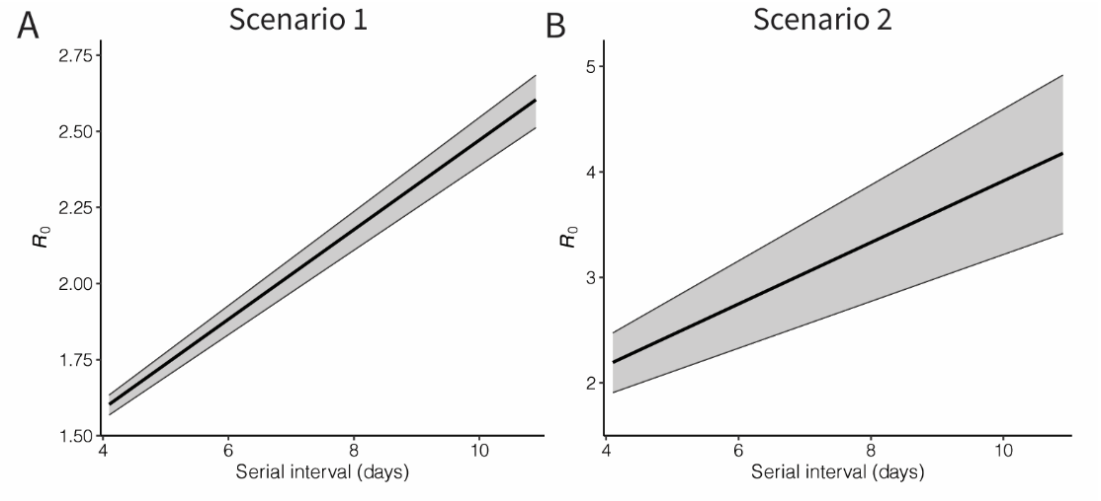

Figure 3. Basic reproduction number of novel coronavirus (COVID-19) infections in China, 2020.

Black lines and grey shades represent the median and 95% credible intervals of the basic reproduction number. Panel A shows the result of Scenario 1, in which an exponential growth started from the assumed illness onset date of the index case, while Panel B shows the result from exponential growth from the first exported case (Scenario 2). The 95% credible intervals were derived from the Markov chain Monte Carlo method.

Discussion

In the present study, we estimated the risk of death of COVID-19 among confirmed cases (cCFR) while accounting for two major biases which may happen in the early stage of the epidemic. First, the underascertainment bias in the reported case counts in China was corrected by using exported cases data diagnosed outside China. We then used a right-censored likelihood in the estimation of risk of death in order to adjust the count of deaths with respect to time delay from illness onset to death. The cCFR was estimated as 5.3% (95% CI: 3.5–7.5) when the date of illness onset for the index case was fixed *a priori* on 8 December 2019 (Scenario 1), and 8.4% (95% CI: 5.3–12.3%) when the timing of the exponential growth of the epidemic was fitted to data along with other model parameters (Scenario 2). In addition, the basic reproduction number (R_0) was estimated in the range of 1.6–2.6 for Scenario 1 and 2.2–4.2 for Scenario 2.

Our main finding suggests that the severity of COVID-19 is not as high as that of other human coronavirus diseases, including SARS which had an estimated CFR of 17% in Hong Kong (Donnelly et al., 2003; Ghani et al., 2005; Nishiura et al., 2009), and Middle East respiratory syndrome (MERS) which had an estimated CFR of 20% in the Republic of Korea (Mizumoto et al., 2015). In addition, given that only approximately 9% of all infected individuals are identified (Nishiura et al., 2020b), the infection fatality risk (IFR; the risk of death among all infected individuals), would be in the range of 0.5% to 0.8%. Nevertheless, considering the massive scale of the ongoing epidemic and the considerable transmissibility of the disease, a 5–8% risk of death among confirmed cases is by no means insignificant. Furthermore, although the heterogeneity in the risk of death was not investigated in the present study, the actual burden of the disease can be substantially amplified if the fatality risk is higher in individuals who are relatively more susceptible to SARS-CoV-2 infections (e.g., individuals with underlying diseases). A more precise risk assessment should be done in the future study once detailed information is made available.

In addition, our estimated R_0 with a range of 2–4 is consistent with other preliminary estimates posted on public domains (Imperial College London-MRC Centre for Global Infectious Disease Analysis, 2020; Read et al., 2021; The University of Hong Kong-HKUMed WHO Collaborating Centre for Infectious Disease Epidemiology and Control; Zhao et al., 2020), and is comparable

to the R_0 of SARS, which was in the range of 2–5 during the 2003 outbreak in Singapore (Lipsitch et al., 2003). These estimates imply that the COVID-19 has substantial pandemic potential, allowing it to spread very rapidly via human-to-human transmission. However, it should be noted that R_0>1 does not guarantee that a single untraced exported case would immediately lead to a major epidemic in the destination country, since the currently planned infectious disease response strategies, including border control and contact tracing with case isolation, could reduce opportunities for transmission to occur (Boldog et al., 2020; Kucharski et al., 2020; Thompson, 2020). In addition, in order to develop an optimal response strategy during the containment stage, the next key question is the presence of presymptomatic transmission, which can determine the importance of intensive contact tracing along with the overall predictability of the ongoing epidemic (Fraser et al., 2004; Thompson et al., 2016).

In both cCFR and R_0, Scenario 2 yielded higher values than Scenario 1, and it is mainly driven by the higher growth rate of incidence (r) in Scenario 2. Considering the uncertainty surrounding the illness onset date of the index case, two different approaches were applied to estimate the growth rate of incidence. However, as the SARS-CoV-2 was sequenced on 7 January 2020, a primer for molecular testing was widely distributed to other countries, resulting in a gradual increase in the number of confirmed cases outside China via a rapid laboratory identification. As a result, the estimates based on Scenario 2, which is fully reliant on the growth rate of exported cases, could be overestimated. On the contrary, the growth rate in Scenario 1 was estimated based on the date of illness onset of the index case, which relies on empirical reports of the earliest onset date for a case. However, the information on the index case is highly likely to be uncertain, particularly in the early stage of the epidemic, thus, the extrapolated exponential growth in Scenario 1 also has a certain level of uncertainty. Nevertheless, we conducted a sensitivity analysis by varying the symptom onset date of the index case in Scenario 1 and ensured that the resulting statistical estimates would not greatly vary from our main results.

Despite the abovementioned limitation, it should be emphasized that the proposed approach can be especially useful for the early risk assessment of newly emerged infectious diseases when local surveillance is likely to be underascertained whereas exported cases and disease-related deaths are better identified. However, extending the use of the proposed method for the COVID-19 epidemic should be done with caution. As all movement in and out of Wuhan (including

international and domestic flights) was banned from 23 January 2020 (BBC NEWS), this intervention abruptly changed the human migration network. Furthermore, despite the decrease in outbound travel from Wuhan, there is a significant risk that other cities will become the next epicenter of SARS-CoV-2 transmissions considering the rapid spread of the disease and the possibility of underreported cases in other regions.

There are three more limitations to be discussed. First, the present study explored the cCFR, which only addresses the risk of death among confirmed cases. For the precise risk assessment, an in-depth understanding of IFR is required based on a better estimation of actual incidences and COVID-19 related deaths. It can be done in a future study when more information becomes available (e.g., seroepidemiological data or outpatient clinic visits for the incidence; excess mortality with pneumonia for the death counts). Second, our study relied on limited empirical data that were extracted from publicly available sources. As all estimates can vary depending on the number of imported cases, future studies with larger samples are needed. Nevertheless, we believe that this study provides critical insight into the situational assessment of the ongoing epidemic. Third, the detection window time T has an uncertainty, which could lead to an overestimated COVID-19 incidence in China. However, since active epidemiological investigations have been implemented outside China, we believe that the sum of the incubation period and the infectious period is a plausible assumption of the detection time window.

In conclusion, the present study has estimated cCFR to be on the order of 5–8% and R_0 to be 1.6–4.2, endorsing the notion that COVID-19 infection in the ongoing epidemic possesses the potential to become a pandemic. The proposed approach can also help direct risk assessment in other settings with the use of publicly available datasets.

Supplementary materials

Sensitivity analysis by varying the starting point of exponential growth of cumulative COVID-19 incidence from 1 December to 10 December 2019

In Scenario 1, the exponential growth of cumulative COVID-19 incidence was assumed to start from the reported illness onset date of the index case (i.e., 8 December 2019), whereas it was allowed to vary in Scenario 2. We conducted a sensitivity analysis by varying the starting date from 1 December 2019 to 10 December 2019 to account for the uncertainty about the illness onset date of the first reported case in Scenario 1. Table S1 and Figure S1 show the estimated growth rate, cumulative incidence, and cCFR for different starting points of the exponential growth.

Table S1. Sensitivity analysis with varying the start point of exponential growth in cumulative incidence with the range of 1–10 December 2019 in estimation Scenario 1.

The start point of exponential growth	Exponential growth rate (95% CI)	Estimated incidence in China on 24 January (95% CI)	cCFR on 24 January (95% CI)
1 December	0.12 (0.11–0.12)	4,718 (3,328–6,278)	5.33% (3.50–7.58)
2 December	0.12 (0.11–0.13)	4,896 (3,473–6,472)	5.35% (3.57–7.61)
3 December	0.12 (0.12–0.13)	5,087 (3,584–6,733)	5.40% (3.59–7.62)
4 December	0.13 (0.12–0.13)	5,392 (3,730–7,024)	5.44% (3.62–7.68)
5 December	0.13 (0.12–0.14)	5,506 (3,908–7,309)	5.48% (3.66–7.74)
6 December	0.14 (0.13–0.14)	5,733 (4,067–7,583)	5.53% (3.68–7.80)
7 December	0.14 (0.13–0.15)	6,089 (4,317–8,099)	5.52% (3.68–7.76)
8 December	0.14 (0.14–0.15)	6,266 (4,435–8,285)	5.64% (3.74–7.96)
9 December	0.15 (0.14–0.16)	6,565 (4,663–8,687)	5.69% (3.79–8.03)
10 December	0.15 (0.14–0.15)	6,924 (4,885–9,211)	5.27% (3.51–7.45)

cCFR: confirmed case fatality risk. CI: confidence interval (the 95% CI was derived from the Markov chain Monte Carlo method). 95% confidence intervals are shown in parenthesis.

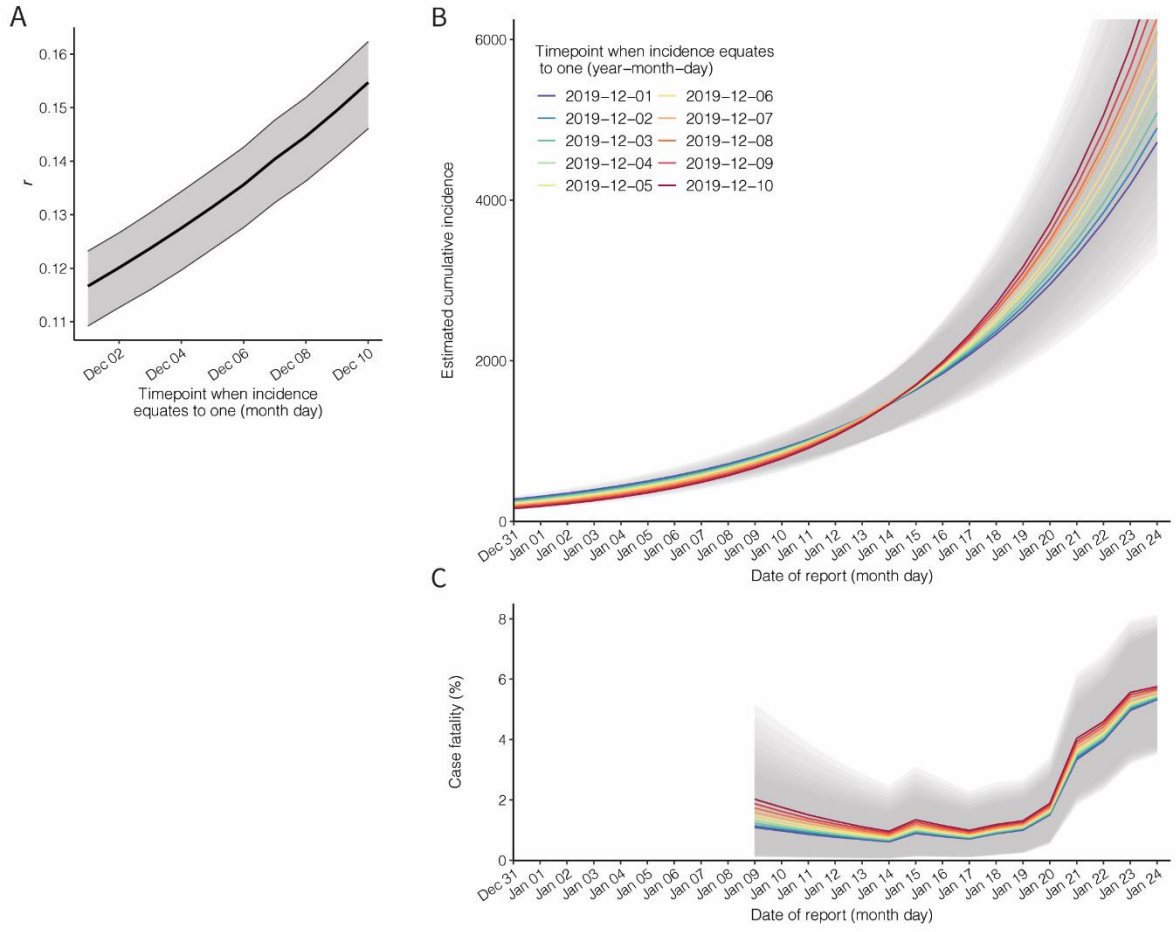

Figure S1. Sensitivity analysis with varied starting points for the exponential growth of cumulative case incidence from 1–10 December 2019.

The estimated values of the: (A) exponential growth rate, (B) cumulative incidence, and (C) confirmed case fatality risk is shown by varying the start date of exponential growth in Scenario 1. Each line and shaded area present the estimate and its 95% confidence interval (derived from the Markov chain Monte Carlo method).

Sensitivity analyses by varying the data cutoff date from 15 January to 24 January 2020

Since the present study relies on real-time data, the estimates (i.e., growth rate, cumulative incidence, and cCFR) using different numbers of cutoff dates are shown in Figure S2 (Scenario 1) and S3 (Scenario 2).

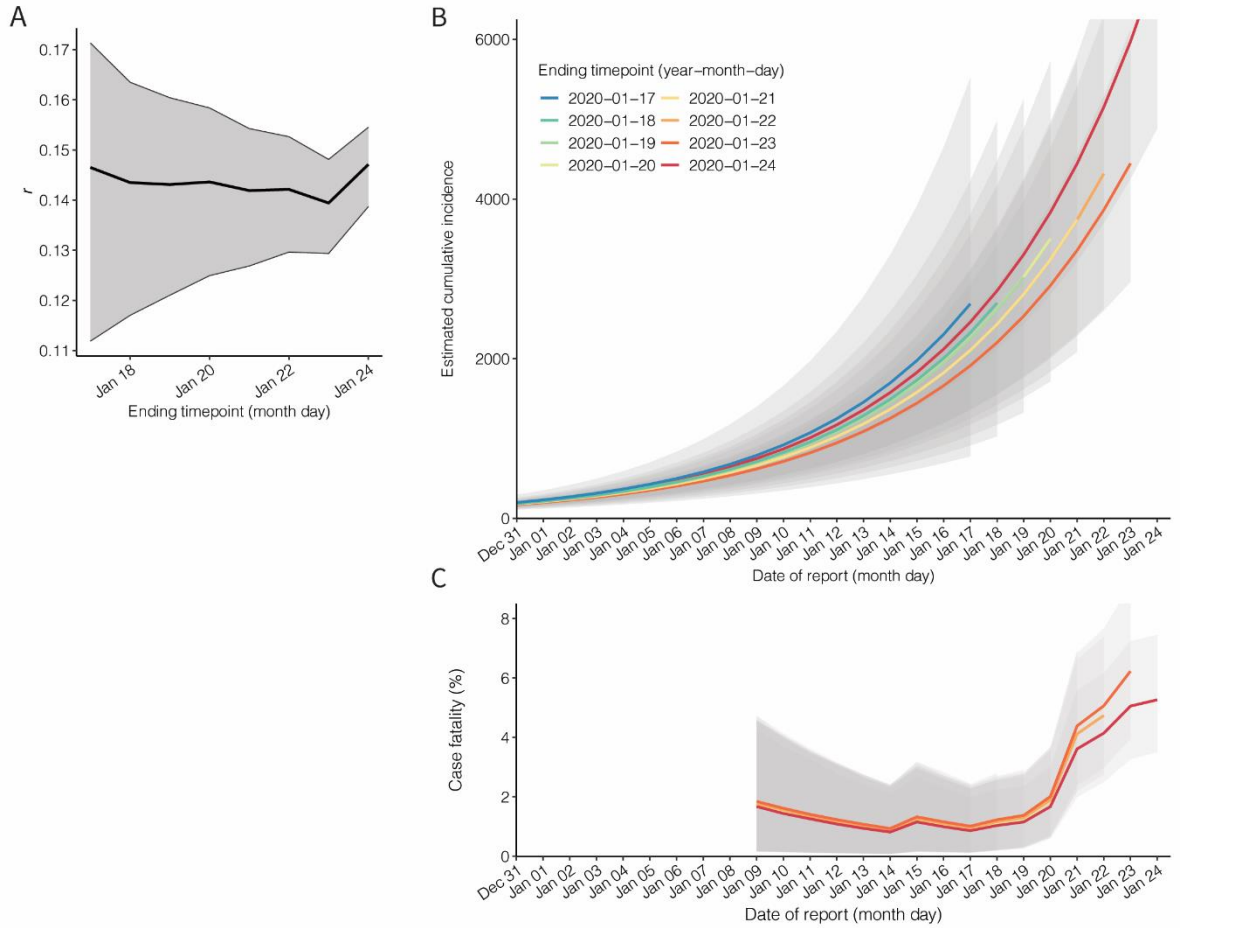

Figure S2. Sensitivity analysis in Scenario 1, varying the data cutoff date between 15 and 24 January 2020.

The estimated values of the (A) exponential growth rate, (B) cumulative incidence, and (C) confirmed case fatality risk depend on the data cutoff date (i.e., the end point of each estimation). Each line and shaded area indicate the estimate and its 95% confidence interval.

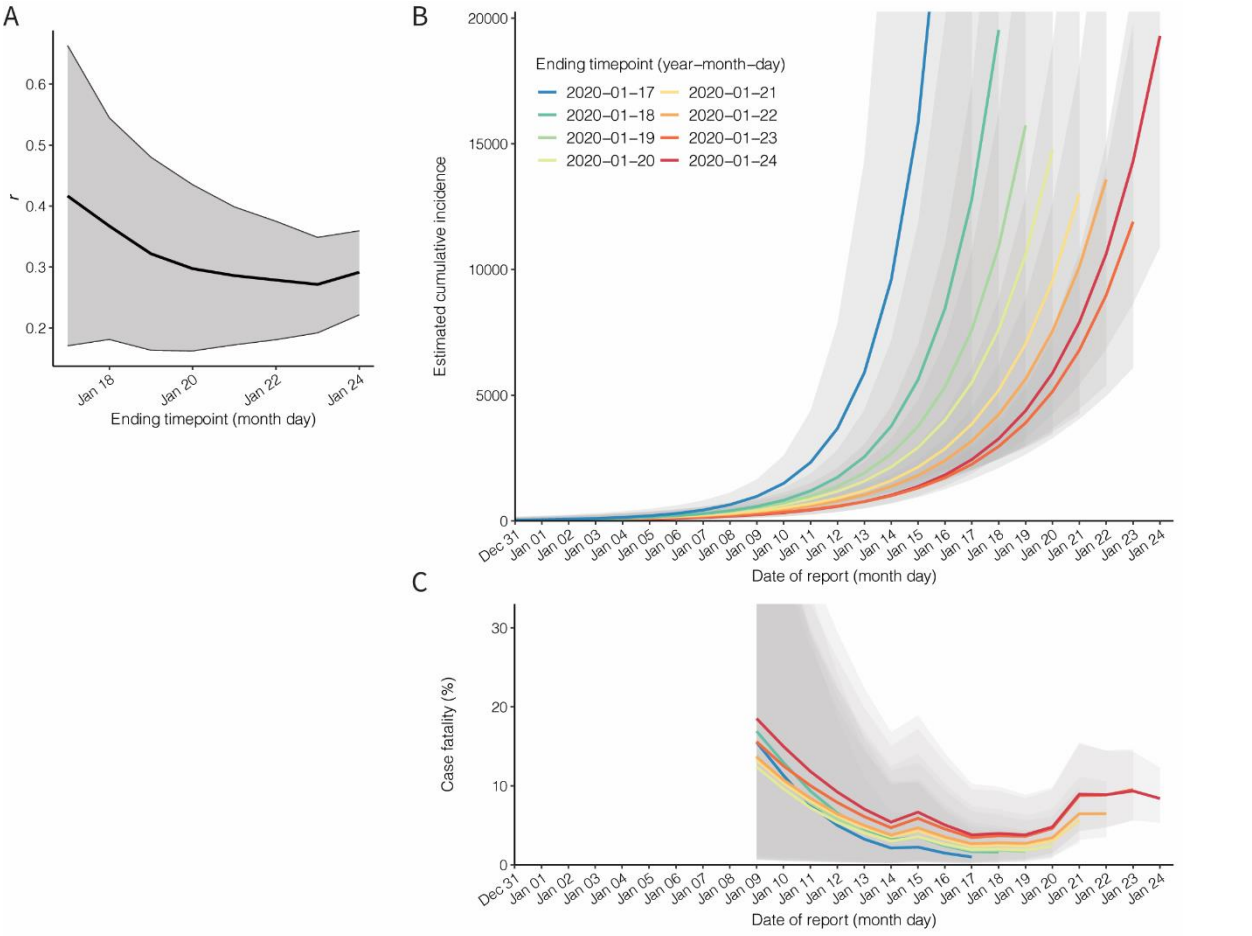

Figure S3. Sensitivity analysis in Scenario 2, varying the data cutoff date between 15 and 24 January 2020.

The estimated values of the (A) exponential growth rate, (B) cumulative incidence, and (C) confirmed case fatality risk depend on the data cutoff date (i.e., the end point of each estimation). Each line and shaded area indicate the estimate and its 95% confidence interval.

Sensitivity analyses by varying the detection time window (T) and catchment population size in Wuhan airport (n)

In the estimation of actual COVID-19 incidence in Wuhan, the detection time window was set at 12.5 days, assuming that the time window is identical to the sum of the incubation period and infectious periods. In addition, the catchment population in Wuhan airport was fixed as 11 million. As part of the sensitivity analysis, Table S2 shows the estimated growth rate, cumulative incidence, and cCFR by varying the detection time window, while Table S3 shows the estimates with different catchment population sizes and a fixed detection time window for Scenarios 1 and 2, respectively.

Table S2. Sensitivity analysis varying the detection time window (T) with a catchment population in Wuhan airport of 11 million

Scenario	Detection window time	Exponential growth rate (95% CI)	Estimated incidence on 24 January (95% CI)	cCFR on 24 January (95% CI)
1	3.6 days	0.18 (0.18–0.19)	30,094(21,524–39,513)	1.82% (1.20–2.58)
1	7.5 days	0.16 (0.15–0.17)	12,024 (8,642–15,838)	3.54% (2.36–4.99)
1	10 days	0.15 (0.14–0.16)	8,343 (5,920–11,040)	4.61% (3.06–6.48)
1	12.5 days	0.15 (0.14–0.15)	6,924 (4,885–9,211)	5.27% (3.51–7.45)
2	3.6 days	0.33 (0.25–0.40)	80,925 (45,517–12,7347)	2.77% (1.72–4.14)
2	7.5 days	0.31 (0.23–0.38)	34,795 (19,653–54,114)	5.31% (3.37–7.87)
2	10 days	0.30 (0.23–0.37)	26,042 (14,602–41,034)	6.64% (4.24–9.82)
2	12.5 days	0.29 (0.22–0.36)	19,289 (10,901–30,158)	8.39% (5.34–12.26)

cCFR: confirmed case fatality risk. CI: confidence interval (the 95% CI was derived from the Markov chain Monte Carlo method). 95% confidence intervals are shown in parenthesis.

Table S3. Sensitivity analysis by varying the catchment population size in Wuhan airport (n) with a fixed detection time window of 12.5 days

Scenario	Catchment population in Wuhan airport	Exponential growth rate (95% CI)	Estimated incidence on 24 January (95% CI)	cCFR on 24 January (95% CI)
1	11 million	0.15 (0.14, 0.15)	6924 (4885, 9211)	5.27% (3.51, 7.45)
1	15 million	0.15 (0.15, 0.16)	9225 (6546, 12187)	4.29% (2.85, 6.04)
1	19 million	0.16 (0.15, 0.17)	12463 (8892, 16416)	3.46% (2.30, 4.88)
2	11 million	0.29 (0.22, 0.36)	19289 (10901, 30158)	8.39% (5.34, 12.26)
2	15 million	0.30 (0.23, 0.37)	27494 (15549, 42771)	6.41% (4.06, 9.49)
2	19 million	0.31 (0.23, 0.38)	36005 (20348, 56273)	5.19% (3.27, 7.68)

cCFR: confirmed case fatality risk. CI: confidence interval (the 95% CI was derived from the Markov chain Monte Carlo method). 95% confidence intervals are shown in parenthesis.

Chapter 1 was originally published as:

Jung S-m, Akhmetzhanov AR, Hayashi K, Linton NM, Yang Y, Yuan B, Kobayashi T, Kinoshita R, Nishiura H. Real-time estimation of the risk of death from novel coronavirus (COVID-19) infection: inference using exported cases. *J Clin Med*. 2020;9(2)523. Minor formatting modifications and edits have been made for the dissertation.

Chapter 2: Projecting a second wave of COVID-19 in Japan with variable interventions in high-risk settings

Background

Since the first imported COVID-19 case was reported on 15 January 2020, the virus rapidly spread to the local community in Japan. (Furuse et al., 2020; The Novel Coronavirus Pneumonia Emergency Response Epidemiology Team, 2020). With the sustained SARS-CoV-2 transmissions, the Japanese government aimed to suppress the epidemic by imposing NPIs based on the "cluster-buster" strategy, which combines active contact tracing with a call for the voluntary reduction of "3C" contacts (i.e., closed spaces, crowded places, and close-contact settings) (Oshitani, 2020). Despite containment efforts with various combinations of NPIs, the number of local cases was upsurged in late March 2020 due to the untraced imported cases (mostly returnees from countries with a high COVID-19 prevalence). In response, the government declared the first state of emergency for seven prefectures (Tokyo, Saitama, Chiba, Kanagawa, Osaka, Hyogo, and Fukuoka) on 7 April 2020, when the country reached a cumulative count of 3,906 COVID-19 cases, excluding 672 cases diagnosed on the Diamond Princess cruise ship (Ministry of Health Labour and Welfare, 2020b); the state of emergency area was later expanded nationwide. In detail, the nightspot-related industries (including bars, restaurants, and host and hostess clubs) were asked to close or to curtail their opening hours, and residents were asked to limit non-household contact on a voluntary basis (i.e., self-restraint-based reduction of physical contact). The state of emergency was initially scheduled to last until 6 May, but this was later extended until 21 May for all prefectures except Hokkaido, Saitama, Chiba, Tokyo, and Kanagawa. The state of emergency was lifted for all prefectures on 25 May 2020 (Ministry of Health Labour and Welfare, 2020a).

In the absence of available prevention or treatment measures (e.g., effective vaccines or antiviral treatments), physical distancing is essential to bring the ongoing epidemic under control. Consequently, many of the most affected areas have requested that their citizens reduce non-essential outings, and some countries even have enforced stringent countermeasures, such as locking down the entire city (Anderson et al., 2020; Gilbert et al., 2020). In Japan, despite that the state of emergency has relied on people's voluntary actions, the incidence of COVID-19 was

greatly reduced shortly after the declaration was issued, easing the burden of the disease on healthcare facilities and public health centers. However, these stringent restrictions on people's lives seen under the state of emergency could not be maintained for an extended period, considering its non-negligible economic, social, and psychological impacts. Thus, the next key questions are whether, when, and to what extent we can maintain socioeconomic activities while sustaining successful suppression of the epidemic. Before effective COVID-19 vaccines become widely available, it is unlikely that sufficient population-level immunity will be established. In addition, despite improvements in the COVID-19 treatment (e.g., treating critically ill patients with dexamethasone) (The RECOVERY Collaborative Group, 2020), a considerable number of deaths have still been documented around the world. Accordingly, resuming the society without proper restraints may lead to a "second wave" of the epidemic in Japan, accompanied by an upsurge in severe cases that may exceed the current capacity of the healthcare system. To avoid such tragedy, a reopening strategy that is balanced between epidemic controls and people's socioeconomic activities needs to be considered. Furthermore, the need of developing such a well-tailored exit strategy might be highlighted even more in countries like Japan where the proportion of immunized individuals is relatively low.

Even after the level of control measures is tapered, physical distancing should remain the primary control measure at least until the healthcare system is well secured by effective pharmaceutical interventions (e.g., nationwide vaccination or utilization of antiviral treatments). However, we could narrow the target of physical distancing such that social functions are minimally affected. Multiple empirical reports have suggested that the transmission of SARS-CoV-2 involves substantial individual-level variation (the majority of cases tend to generate no or only a few secondary transmissions), implying that the current epidemic is mainly driven by "superspreading events" (defined as an unusually large number of secondary cases infected by a single individual in a short period). In addition, since such uneven transmissions have been frequently observed in specific settings with 3C contacts (Liu et al., 2020; Nishiura et al., 2020c), stringent control measures were imposed primarily on settings they deem to be high-risk in most countries (e.g., restaurants, and bars, and mass gathering events) (Ministry of Health Singapore, 2020). Therefore, if we focus intervention efforts on such high-risk settings and minimize the risk of superspreading events, we may be able to bring the epidemic under control while

allowing other parts of society to gradually resume a normal life. Such a political decision should be guided by quantitative assessment, comparing different targets and levels of interventions.

In this respect, projections of future waves using a mathematical modelling approach can provide valuable insight into an optimal exit strategy. Thus, the present analysis aimed to assess the impacts of possible exit strategies for two of the most populous regions in Japan (i.e., Tokyo Metropolis and Osaka prefecture), classifying the population into high- and low-risk settings. Using the estimated growth rates of COVID-19 incidence, we quantified the risk-based next-generation matrix and projected future epidemic scenarios with different levels of restriction.

Methods

Epidemiological data

The daily incidence of confirmed COVID-19 cases in Tokyo and Osaka were retrieved from 24 January (the earliest date of case reporting in Tokyo) through 26 May 2020. In detail, information on those cases, including dates of illness onset and laboratory confirmation, were obtained from the Ministry of Health, Labour and Welfare (Ministry of Health Labour and Welfare, 2020c) and from prefectural government websites (Osaka Prefectural Government, 2020; Tokyo Metropolitan Government, 2020a). A total of 6,540 confirmed symptomatic COVID-19 cases were included, whereas a total of 26 symptomatic cases with neither report of illness onset date nor laboratory confirmation date were excluded from the dataset.

Back-projection

The dates of illness onset for 915 and 22 confirmed symptomatic cases in Tokyo and Osaka, respectively, were unknown. Therefore, the onset date of these cases was back-projected from the date of laboratory confirmation using the empirically observed delay distribution between these dates. First, we fitted the right-truncated time delay from illness onset to laboratory confirmation, employing a Weibull distribution. The likelihood was defined as:

$$L(\theta|S_k, O_k, T) = \prod_{k=1}^{K} \frac{h(S_k - O_k|\theta)}{H(T - O_k|\theta)}, \quad (1) \qquad \textbf{(10)}$$

where S_k is the date of laboratory confirmation of case *k*, O_k is the date of illness onset of case *k*, and T is the latest calendar date of observation (27 May 2020). The functions $h(\cdot)$ and $H(\cdot)$ are the probability mass function and the cumulative distribution function of the Weibull distribution, respectively, and θ is the set of relative parameters (i.e., shape and scale parameters). The best-fit parameters were determined by maximizing the likelihood to be used in the back-projection.

Second, using the parameterized delay distribution and the R package '*surveillance*' (Höhle, 2007), based on the non-parametric back-projection algorithm, all cases with unknown illness onset dates were back-projected. The back-projected cases by date of onset were then aggregated with cases with known dates of onset. We also accounted for the right-censoring with respect to the time delay from illness onset to laboratory confirmation. The "nowcasted" number of new cases with the date of illness onset *t* ($i(t)$) was calculated as:

$$i(t) = \frac{i_{\text{reported}}(t)}{H(T-t)}, \tag{11}$$

where $i_{\text{reported}}(t)$ is the number of newly reported cases on date *t*. In the analysis, the nowcasted incidence for the latest 3 days was unreliable because the value of $H(\cdot)$ was too small; therefore we excluded these dates (24 May 2020 onward) from the analysis.

Model and statistical analysis

We then conducted the projection analysis relying solely on the nowcasted date of illness onset. Our main model consisted of three components: (i) exponential fitting, (ii) offspring distribution fitting, and (iii) next-generation matrix reconstruction. First, we fitted the exponential increase function to the observed case counts to estimate the time-dependent reproduction numbers. We then constructed offspring distributions corresponding to the estimated reproduction numbers and approximated them by a mixture of two distributions for two types of hosts: low- and high-risk transmission settings. Finally, using the median value for the two types of hosts, the next generation matrix was reconstructed.

Estimation of exponential growth rates

Let $i(t)$ be the incidence of infection (i.e., the number of newly infected individuals at time t). Given the constant next-generation matrix, we expect that $i(t)$ will converge to an exponential curve. We split the time axis into multiple periods (e.g., Period 1 $[t_0 < t < t_1]$, Period 2 $[t_1 < t < t_2]$), during which the next generation matrix K_n $(n = 1, 2, \ldots)$ was assumed to stay constant, and we assumed that $i(t)$ in each period would swiftly converge to the asymptotic exponential curve such that $i(t)$ is well approximated by joint exponential curves:

$$i(t) = i_{n(t)-1} \exp\left(r_{n(t)} t\right), \tag{12}$$

where $n(t)$ represents the period number to which t belongs (i.e., $t_{n(t)} < t < t_{n(t)+1}$), and r_n is the growth rate during Period n. The value of $i(t)$ at the beginning of Period n is represented by $i_{n-1} = i(t_{n-1})$. Because we observe incidence using onset j_t rather than infection $i(t)$ itself, the observation is delayed by the incubation period (whose relative frequency is represented by $f(\tau)$). The corresponding likelihood function is therefore:

$$L(\boldsymbol{r}; \boldsymbol{j}) = \prod_t \mathrm{Pois}\left(j_t; (i * f)(t)\right), \tag{13}$$

where $(i * f)(t) = \sum_{\tau=1}^{t} i(t - \tau) f(\tau)$ represents the expected incidence of illness onset. The values of the incubation period distribution ($f(\tau)$) were adopted from a previous study (mean = 5.6 days, standard deviation = 3.9 days) (Linton et al., 2020).

We used the following three time periods: (i) the early invasion period (before 26 March 2020 for Tokyo and before 18 March 2020 for Osaka), (ii) the period after an alert was declared by the prefectural governor of each region (26 March–7 April 2020 for Tokyo and 19 March–7 April 2020 for Osaka) and (iii) the period after the governmental declaration of a state of emergency (8 April–25 May 2020 for Tokyo and 8 April–21 May 2020 for Osaka). We fitted our model to the back-projected incidence by onset through 23 May 2020. The growth rates for the three periods (r_1, r_2, and r_3) were estimated by the Markov chain Monte Carlo (MCMC) method. Instead of directly sampling r_1, r_2 and r_3, we sampled $i(t)$ at the change points (i.e. i_n [n = 0, 1, 2, 3]), the logarithms of which had improper flat priors ($\log(i_n) \approx \mathrm{Unif}(-\infty, \infty)$). We ran 200,000 MCMC iterations to obtain 2,000 thinned samples, and we discarded the first half as burn-in. We

confirmed that the effective sample size of the resulting 1,000 MCMC samples was larger than 500 for all parameters. The sampled i_n was then translated to r_n as:

$$r_n = \left(\frac{i_n}{i_{n-1}}\right)^{-(t_n - t_{n-1})}. \quad (14)$$

We used *R* program (version 3.6.2) and the "*LaplacesDemon*" package to implement the MCMC (version 16.1.4).

Approximation of the offspring distribution

Assuming that the generation time follows a gamma distribution with a mean (T) of 4.8 days and a coefficient of variation (v) of 0.5 days (Nishiura et al., 2020d), we can obtain the converted value of the effective reproduction number from the growth rate using the Euler–Lotka equation (Nishiura et al., 2009; Wallinga and Lipsitch, 2007):

$$R_n = (1 + r_n T v^2)^{\frac{1}{v^2}}. \quad (15)$$

The offspring distribution of COVID-19, defined as the distribution of the number of secondary transmissions reproduced by a single primary case, has previously been modelled using a negative binomial distribution with the most plausible value of the overdispersion parameter $k \approx 0.1$ (Endo et al., 2020). The mean of the negative binomial distribution, by definition, corresponds to the reproduction number. We assumed that the overdispersion parameter remains constant regardless of the reproduction number (i.e., the coefficient of variation is conserved) and that such a negative binomial distribution can be approximated as a mixture of two offspring distributions corresponding to low- and high-risk transmission subgroups:

$$\hat{p}(x) = a p_L(x) + (1 - a) p_H(x), \quad (16)$$

where a is the mixture proportion (i.e., the proportion of the total secondary transmissions that are low-risk transmissions). Let R_L and R_H ($R_L < R_H$) represent the mean values of $p_L(x)$ and $p_H(x)$, respectively.

For each of the negative binomial offspring distributions corresponding to different reproduction numbers R_n (n = 1, 2 and 3):

$$p_n(x) = \mathrm{NegBin}(k = 0.1, \mathrm{mean}\ = R_n), \tag{17}$$

we estimated the mixture distributions $\hat{p}(x)$ that provide the best approximation, where $p_L(x)$ and $p_H(x)$ are both assumed to be geometric distributions. We measured the deviation between $\hat{p}(x)$ and $p(x)$ by the Kullback–Leibler (KL) divergence (truncated at x = 300 for computational convenience):

$$D_{\mathrm{KL}}(p(x)||\hat{p}(x)) = \sum_{x=0}^{300} p(x)\log\left(\frac{p(x)}{\hat{p}(x)}\right), \tag{18}$$

and we minimized this value to find the best $\hat{p}(x)$. We obtained the two means, R_L and R_H, for each MCMC sample for each period (n = 1, 2, and 3). We ensured that the minimized value of the KL divergence was less than 0.01. We used Julia-1.4.1 and the "*Optim.jl*" package for optimization, which were called from R with Version 0.17.1 of the "*JuliaCall*" package.

Reconstruction of the next generation matrix

From the mean values R_L and R_H, corresponding to the low- and high-risk transmission subgroups, we reconstructed the next generation matrix. The two-by-two next-generation matrix $K = (k_{ij})$ is expected to satisfy the following conditions: (i) the column sums are equal to R_L and R_H, (ii) the eigenvalue of the matrix corresponds to R_n, and (iii) the off-diagonal entries of K satisfy $qk_{LH} = (1 - q)k_{HL}$, where q represents the relative size of contact in the high-risk subgroup (assuming that the risk of transmission is proportional to the contact rate). To ensure that the estimated next-generation matrix is positive-definite, we found that the parameter value of q has to be within the range of 0–0.01 given the value of a, R_L, and R_H in Period 1 (See Appendix 1). Thus, the value of q was assumed to be 0.01 in the main analysis, and a sensitivity analysis was carried out adopting a smaller value of q (0.001).

Let R and ρ be the two eigenvalues of K (i.e., $R > \rho$) and $V = \begin{pmatrix} a & b \\ 1-a & 1-b \end{pmatrix}$ be the corresponding eigenvector matrix. We can then decompose K as

$$K = \begin{pmatrix} a & b \\ 1-a & 1-b \end{pmatrix}\begin{pmatrix} R & 0 \\ 0 & \rho \end{pmatrix}\begin{pmatrix} a & b \\ 1-a & 1-b \end{pmatrix}^{-1}, \tag{19}$$

where a, b and ρ are unknowns to be determined by the binding conditions: $R_L = k_{LL} + k_{HL}$ and $R_H = k_{LH} + k_{HH}$. From condition (ii), we get

$$R_L = \frac{(1 - b)R - (1 - a)\rho}{a - b},$$
$$R_H = \frac{a\rho - bR}{a - b} \tag{20}$$

When we fix a as a constant, the above simultaneous equations for (ρ, b) have a solution if and only if $R = aR_L + (1 - a)R_H$. Suppose the value of a satisfies this condition; such an a corresponds to that in Equation (16). Under such conditions, the two equations in (20) are reduced to a single equation:

$$\rho = R_H - b(R_H - R_L). \tag{21}$$

In addition, to satisfy condition (iii), we require

$$(1 - q - a)b = (1 - a)(1 - q), \tag{22}$$

which only has a solution when $q \neq 1 - a$. We solved the simultaneous equations given by Equations (21) and (22) and obtained K from Equation (19) for each MCMC sample.

Projection of newly reported cases

For the future projections, four different scenarios were considered: Scenario 1, going back to the pre-emergency period (i.e., assuming the next-generation matrix resumes, taking on values observed in Period 1), and Scenarios 2−4, with 10%, 30%, and 50% decreases in high-risk transmission (i.e., assuming the normal low-risk transmission rate [k_{LL} and k_{HL}] but a 10%, 30%, or 50% decrease in the high-risk transmission rate [k_{LH} and k_{HH}]). Thus, in the scenarios assuming a decrease in high-risk transmission, the low-risk transmission fully returns to the original level from 21 May 2020 and 25 May 2020 in Osaka and Tokyo, respectively, whereas the high-risk transmission is partially suppressed.

Using the growth rates in each scenario derived from the adjusted next-generation matrices, the number of newly infected cases at time *t*, $i(t)$, was projected for each city as an exponential curve, and the expected incidence by the date of illness onset *t* was calculated as:

$$E(j_t) = \sum_{\tau=1}^{t} i(t - \tau) f(\tau). \quad (23)$$

The median and 95% credible intervals (CrI) were produced from the MCMC samples.

In order to compare our projection with the actual post-projection incidence, the reported number of cases by the date of illness onset during the projection period (25 May–30 July 2020 for Tokyo; 21 May–30 July 2020 for Osaka) was back-projected from the date of laboratory confirmation. However, it should be noted that since the information of the date of illness onset of all cases in Tokyo was not available from June onwards, this post-projection data no longer represents the same data source as the data used for projection, which may have caused a small discrepancy in incidence at the connecting point in the time series (Figure 4).

Results

Table 2 demonstrates the quantified next-generation matrix (*K*) for each time period in Tokyo and Osaka. The effective reproduction numbers for Tokyo were estimated as 1.78 (95% CrI: 1.73–1.82) in Period 1, 0.74 (95% CrI: 0.71–0.78) in Period 2, and 0.63 (95% CrI: 0.61–0.65) in Period 3. In Osaka, although the estimated reproduction number in Period 2 (i.e., after the request for self-restraint from the governor of Osaka) declined compared with that in Period 1 (1.58 [95% CrI: 1.51–1.64]), the estimated value in Period 2 was still above one (1.20 [95% CrI: 1.15–1.25]). In Period 3, the reproduction number was estimated at 0.48 (95% CrI: 0.44–0.51). Transmission rates from low-risk subgroup to low-risk subgroup (k_{LL}) in both regions (Tokyo and Osaka) were essentially constant across all three time periods, while the other three transmission rates (k_{LH}, k_{HL}, and k_{HH}) in Period 3 were less than half of their Period 1 rates. In addition, the estimated next-generation matrices produced very similar results in the analysis excluding cases with unknown dates of illness onset.

Figure 4 shows the projection of new infections and cases in Tokyo and Osaka. In Tokyo, the projected number of newly infected cases in Scenario 1, assuming the same reproduction number as in Period 1 (R_1 = 1.78), showed a rapid resurge after the reopening the society on 26 May and reached the same value as the peak incidence during the pre-reopening period (i.e., 223 cases) on 4 July 2020. The estimated reproduction numbers in Scenarios 2 and 3 were 1.62 (95% CrI: 1.58–1.66) and 1.30 (95% CrI: 1.27–1.33), respectively, also indicating resurgence. However, in Scenario 4 (assuming a 50% decrease in high-risk transmission), the estimated reproduction number was below the value of one (0.98 [95% CrI: 0.95–1.00]), and the projected epidemic was on the verge of dying out (Figure 4A). Likewise, in Osaka, only Scenario 4 could prevent a resurgence of cases; with all reported cases, the estimated reproduction numbers for Scenarios 2, 3, and 4 were 1.44 (95% CrI: 1.38–1.49), 1.16 (95% CrI: 1.11–1.20) and 0.87 (95% CrI: 0.84–0.90), respectively. The projected numbers of new cases by date of illness onset were aligned with the overall trend of observed case counts, as shown in Figures 4B and 4D, implying that our model accurately reconstructed COVID-19 transmission dynamics in both regions. In particular, the reported number of cases in Tokyo during the projected period was consistent with Scenario 1, while those in Osaka exceeded all our projections.

Table 2. Estimated next-generation matrix of COVID-19 by time period in Tokyo Metropolis and Osaka, Japan

Region	Period 1*		Period 2		Period 3	
Including back-projected cases						
Tokyo Metropolis	k_{LL} = 0.02 (0.02–0.02)	k_{LH} = 6.09 (5.97–6.21)	k_{LL} = 0.03 (0.03–0.03)	k_{LH} = 3.08 (2.98–3.19)	k_{LL} = 0.03 (0.03–0.03)	k_{LH} = 2.70 (2.63–2.77)
	k_{HL} = 0.06 (0.06–0.06)	k_{HH} = 1.56 (1.52–1.60)	k_{HL} = 0.03 (0.03–0.03)	k_{HH} = 0.61 (0.58–0.64)	k_{HL} = 0.03 (0.02–0.03)	k_{HH} = 0.51 (0.49–0.53)
	R_1 = 1.78 (1.73–1.82)		R_2 = 0.74 (0.71–0.78)		R_3 = 0.63 (0.61–0.65)	
Osaka Prefecture	k_{LL} = 0.02 (0.02–0.02)	k_{LH} = 5.55 (5.37–5.72)	k_{LL} = 0.02 (0.02–0.03)	k_{LH} = 4.49 (4.34–4.63)	k_{LL} = 0.03 (0.02–0.03)	k_{LH} = 2.18 (2.04–2.30)
	k_{HL} = 0.06 (0.05–0.06)	k_{HH} = 1.38 (1.32–1.44)	k_{HL} = 0.05 (0.04–0.05)	k_{HH} = 1.03 (0.98–1.07)	k_{HL} = 0.02 (0.02–0.02)	k_{HH} = 0.38 (0.34–0.41)
	R_1 = 1.58 (1.51–1.64)		R_2 = 1.20 (1.15–1.25)		R_3 = 0.48 (0.44–0.51)	
Excluding cases with an unknown illness onset						
Tokyo Metropolis	k_{LL} = 0.02 (0.02–0.02)	k_{LH} = 5.99 (5.87–6.10)	k_{LL} = 0.03 (0.03–0.03)	k_{LH} = 2.94 (2.83–3.05)	k_{LL} = 0.03 (0.03–0.03)	k_{LH} = 2.85 (2.77–2.92)
	k_{HL} = 0.06 (0.06–0.06)	k_{HH} = 1.53 (1.49–1.57)	k_{HL} = 0.03 (0.03–0.03)	k_{HH} = 0.57 (0.54–0.61)	k_{HL} = 0.03 (0.03–0.03)	k_{HH} = 0.55 (0.53–0.57)
	R_1 = 1.74 (1.69–1.78)		R_2 = 0.70 (0.67–0.73)		R_3 = 0.67 (0.65–0.70)	
Osaka Prefecture	k_{LL} = 0.02 (0.02–0.02)	k_{LH} = 5.58 (5.39–5.75)	k_{LL} = 0.03 (0.03–0.03)	k_{LH} = 4.21 (4.07–4.35)	k_{LL} = 0.03 (0.03–0.03)	k_{LH} = 2.35 (2.22–2.48)
	k_{HL} = 0.06 (0.05–0.06)	k_{HH} = 1.39 (1.32–1.45)	k_{HL} = 0.04 (0.04–0.04)	k_{HH} = 0.94 (0.90–0.99)	k_{HL} = 0.02 (0.02–0.03)	k_{HH} = 0.42 (0.39–0.45)
	R_1 = 1.59 (1.52–1.65)		R_2 = 1.10 (1.06–1.15)		R_3 = 0.53 (0.49–0.56)	

The values of k_{ij} describe the transmission rates from group *j* to group *i*, and R_n is the reproduction number in Period *n* derived from the estimated next-generation matrix. Upper and lower 95% credible intervals obtained from the MCMC samples are shown in parentheses.

*Three time periods were (1) the early invasion period (before 26 March 2020 for Tokyo and before 18 March 2020 for Osaka), (2) the period after an alert was declared by the prefectural governor of each region (26 March–7 April 2020 for Tokyo and 19 March–7 April 2020 for Osaka) and (3) the period after the governmental declaration of a state of emergency (8 April–25 May 2020 for Tokyo and 8 April–21 May 2020 for Osaka).

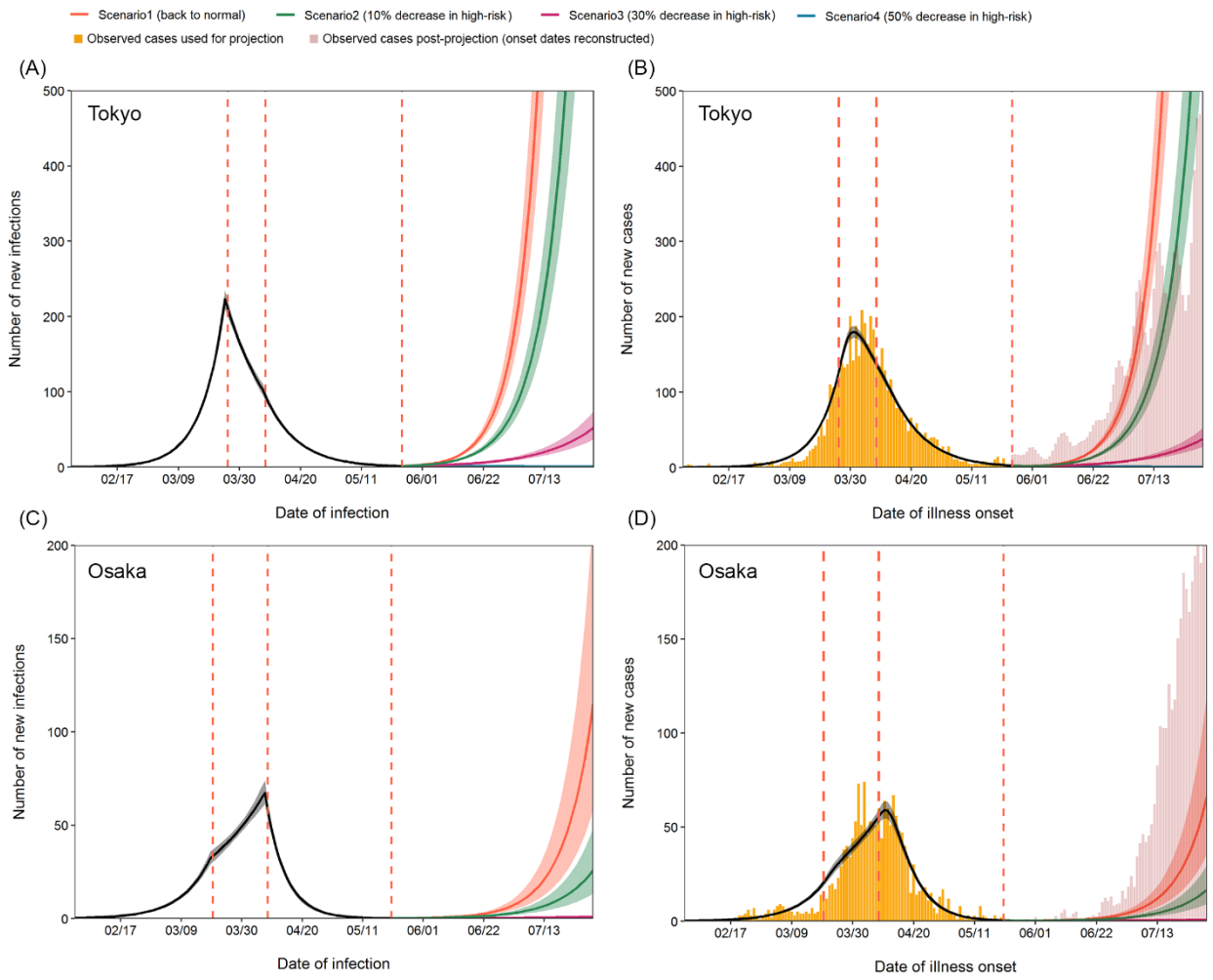

Figure 4. Estimated and projected trajectories of COVID-19 cases by date of infection and symptom onset including cases with unknown illness onset dates in Tokyo and Osaka, Japan.

(A) (C) Estimated and projected numbers of COVID-19 cases by date of infection in Tokyo and Osaka, using all back-projected cases (yellow bars). The temporal trend in the number of new infections by 31 May 2020 was estimated using exponential curves with three different growth rates (black) and was then projected according to four scenarios (colors). The lines denote medians, and shaded areas represent 95% credible intervals (CrI). Red dotted lines denote the dates when we assumed the trend changed (26 March, 8 April, and 25 May 2020 for Tokyo; 20 March, 8 April, and 21 May 2020 for Osaka) (B) (D) Observed, estimated, and projected numbers of COVID-19 cases by date of illness onset in Tokyo and Osaka. Yellow bars show the observed number of cases by the date of illness onset used for the projection, and red bars show

the observed number of cases in the post-projection period (25 May–30 July 2020 for Tokyo; 21 May–30 July 2020 for Osaka). A small inconsistency was observed at the connecting part between the two time series because the post-prediction data lacked dates of illness onset, which were thus all reconstructed by the back-projection method from dates of laboratory confirmation. The estimated (black) and projected (colors) numbers of cases and their 95% CrI are shown as lines and shaded areas, respectively.

Figure 5 shows the projected number of new infections and cases obtained from the dataset excluding cases with unknown illness onset. The estimated reproduction numbers in Scenarios 2, 3, and 4 in Tokyo were 1.58 (95% CrI: 1.54–1.62), 1.27 (95% CrI: 1.24–1.30) and 0.96 (95% CrI: 0.93–0.98), respectively, whereas those in Osaka were estimated as 1.45 (95% CrI: 1.38–1.50), 1.16 (95% CrI: 1.11–1.21) and 0.88 (95% CrI: 0.84–0.91), respectively.

Throughout the sensitivity analyses, only the scenario with a 50% decrease in high-risk transmission was able to keep the reproduction number below one (Table S1). Our conclusions did not change significantly even with the relative size of the high-risk subgroup (q) set to a smaller value of 0.001 (as opposed to 0.01 in the main analysis). All entries related to the high-risk transmission rates (k_{LH} and k_{HH}) showed very similar values. Although the values of k_{HL} and k_{LL} changed slightly, the effects on the results were minor (Table S2). In addition, the sensitivity was evaluated by varying the overdispersion parameter (k) in the range of 0.05–0.2, taking into account the uncertainty of this parameter (Gilbert et al., 2020). Decreasing k values (i.e., high dispersion in the offspring distribution) were associated with larger estimated entries for high-risk transmission rates (k_{LH} and k_{HH}), which could indicate that reducing high-risk transmission is particularly important in diminishing transmission when the number of secondary transmissions varies widely between individuals (Tables S3 and S4).

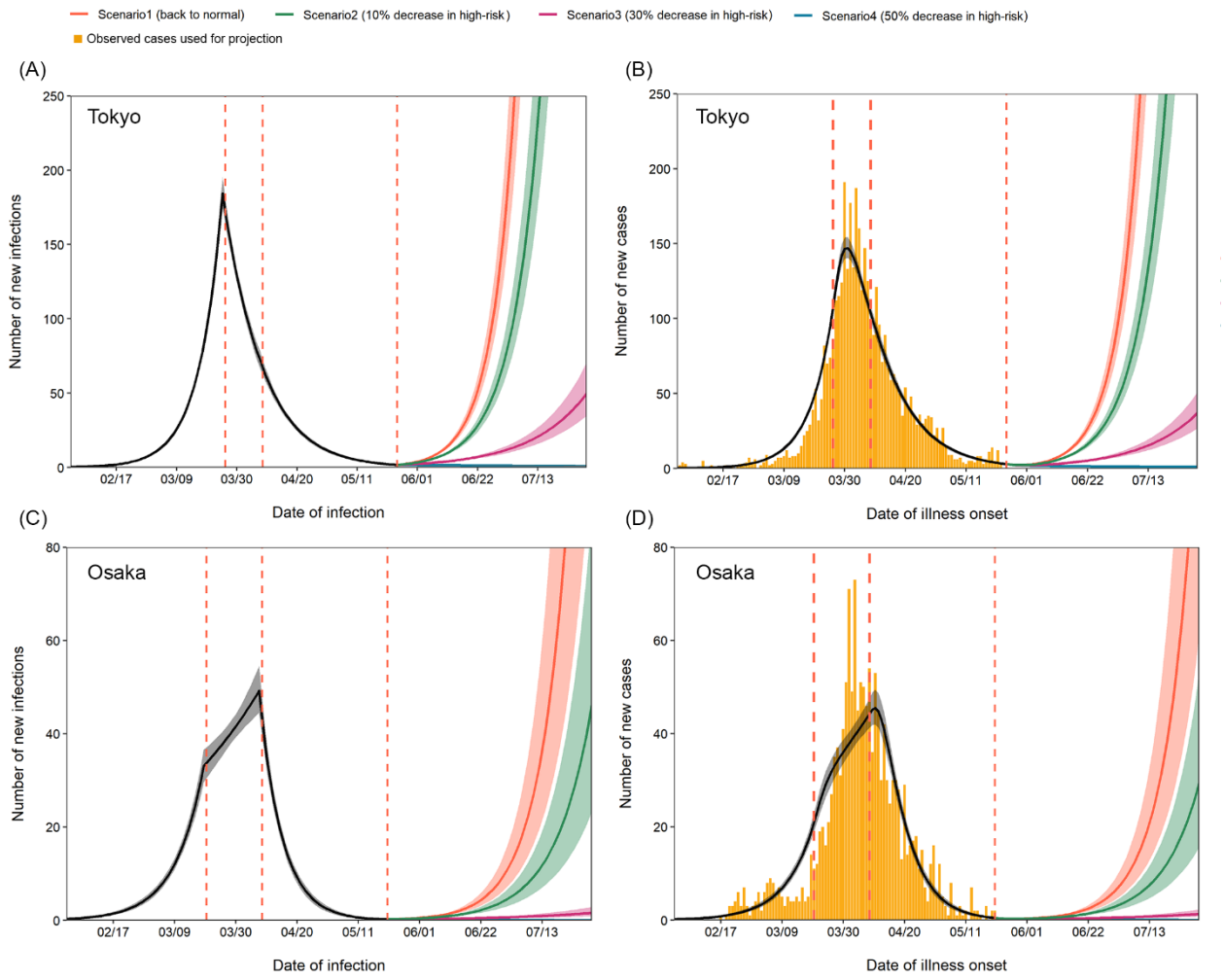

Figure 5. Estimated and projected trajectories of COVID-19 cases by date of infection and symptom onset, excluding cases with unknown illness onset in Tokyo and Osaka, Japan.

(A) (C) Estimated and projected numbers of COVID-19 cases by date of infection without back-projected cases in Tokyo and Osaka. The temporal trend in the number of new infections by 31 May 2020 was estimated using exponential curves with three different growth rates (black) and was then projected according to four scenarios (colors). The lines denote medians, and shaded areas represent 95% credible intervals (CrI). Red dotted lines denote the dates when we assumed the trend changed (26 March, 8 April, and 25 May 2020 for Tokyo; 20 March, 8 April, and 21 May 2020 for Osaka). (B) (D) Observed, estimated, and projected numbers of COVID-19 cases by date of illness onset in Tokyo and Osaka. The bars show the observed number of cases by illness onset. The estimated (black) and projected (colors) numbers of cases and their 95% CrI are shown as lines and shaded areas, respectively.

Discussion

In the present study, we quantified the next-generation matrices classifying the population into low- and high-risk transmission settings, and projected the future trend of SARS-CoV-2 infections in Tokyo and Osaka after lifting the first state of emergency on 26 May 2020. Among four scenarios with different levels of reduction in high-risk transmission, only the one with a 50% reduction (Scenario 4) was able to achieve containment of the epidemic ($R_4 < 1$), whereas other scenarios with smaller reductions resulted in a resurgence. In Tokyo, under the 'back to normal' scenario (Scenario 1), the projected number of daily new cases in early July 2020, including all back-projected cases, was already as large as the peak (209 cases) observed on 3 April 2020. The number of new cases is likewise projected to increase under the 10%- and 30%-reduction scenarios, given that the reproduction number in each scenario is above one. The estimated reproduction number in Osaka was also above one in each scenario except Scenario 4, with a 50% decrease in high-risk transmission.

The projected number of COVID-19 cases under the 'back to normal' scenario was in line with the overall trend of observed case counts in Tokyo. After the nationwide interventions under the state of emergency were lifted on 25 May 2020 without any intervention in high-risk settings, several nightspots-related clusters (mainly in host and hostess clubs) aided in the resurge of COVID-19 incidence in Tokyo, which was likely to have resulted in a similar growth as Scenario 1. Furthermore, as nightspots-related clusters tend to pose special difficulties to the contact tracing in practice, those clusters have triggered additional local-level transmissions in Tokyo (e.g., transmissions in households and workplaces). From around the middle of July, the observed growth of cases slowed down compared to the projection, which might correspond with the Tokyo governor's request for the residents to avoid high-risk settings and implementation of intensive PCR testing targeted for individuals in nightspots in early July (Shinjyuku City, 2021; Subcommittee on Novel Coronavirus Disease Control, 2020; Tokyo Metropolitan Government, 2020c, 2020b). On the other hand, the observed post-projection incidence was higher than any of the projected scenarios in Osaka. The effective reproduction number estimated from the observed case counts was around the value of two from mid-June to mid-July 2020 in Osaka (Subcommittee on Novel Coronavirus Disease Control, 2021), which was higher than our assumed reproduction number $R_1 = 1.6$ (the value we estimated from the initial growth). One

possible explanation for such discrepancy could be a behavior change. Since there were multiple reports of large-size clusters in Osaka (e.g., four live-house-related clusters) in March, the risk awareness of Osaka residents may have already been elevated in Period 1, resulting in their contact behavior and transmission risk being higher in the post-emergency period (National Institute of Infectious Diseases, 2020).

Our main finding suggests that a decrease of more than 50% in the high-risk transmission is necessary to reduce the reproduction number of COVID-19 below unity. This can be theoretically supported by the concept of type-reproduction number, T (Heesterbeek and Roberts, 2007), and the value of 50% is indeed consistent with $1 - 1/T$ for the high-risk group, which would be slightly more challenging than $1 - 1/R_1 = 1 - 1/1.7 = 41.2\%$. Although defining the precise range of high-risk settings can be challenged in practice, these results imply that before the population-level immunity is established, full-reopening of society may lead to the second wave of COVID-19, and essential groups of hosts should thus be targeted for control to sustain low levels of transmission. A temporary resurgence may be observed even with the 50% of reduction in high-risk transmission because of the stochasticity of transmission dynamics. Nevertheless, the exit strategy from restrictive guidelines should aim for the reproduction number of COVID-19 below one because it would ensure the eventual extinction or at least continued suppression of the disease (Jacquez and O'Neill, 1991).

In addition, the number of cases under the 30%- reduction scenario (Scenario 3) would be much lower than the 'back to normal' scenario (Scenario 1), and it might be viewed as a possible exit strategy in terms of minimizing the economic loss. However, it should be noted that not only the absolute number of COVID-19 cases, but also its ensuing burdens on healthcare settings (e.g., contact tracing, molecular testing, and nosocomial isolation) should all be taken into account when determining the exit strategy. Furthermore, even after the disease burden may be substantially reduced once effective antiviral treatments are developed, minimizing the disease incidence should continue to be prioritized, considering the "long COVID" syndrome (i.e., long-lasting COVID-19 symptoms after the recovery from infection). For more precise evaluation, a future study should assess the cost-effectiveness of possible exit strategies, considering both the economic loss associated with the social distancing in high-risk settings and the overall disease burden.

We approximated the overall offspring distribution, characterized as a negative binomial distribution, using a mixture of two geometric distributions with mean values of 0.08 and 7 for Period 1. The next-generation matrix reconstructed from these mean values was interpretable (i.e., positive values for all entries) only when the proportion at high risk (q) was very small ($q < 0.015$). This may indicate that the high-risk subgroup, generating seven secondary cases on average, would have to be disproportionately small in the population to be consistent with the observed reproduction number of 1.5. However, the proportion made up by the high-risk subgroup is larger in the infected population because of this population's relatively high risk of infection. In the approximated mixture offspring distribution, the high-risk subgroup accounted for 20% (according to the estimated value of a) of infectors and was responsible for 96% of the overall secondary transmissions. Although these are merely interpretations of the results of our mixture approximation and are not directly based on empirical data, our results suggest that a very small fraction of high-risk transmission could lead to a growing epidemic, as we observed in our projections. Thus, focusing on suppressing transmission in high-risk settings might have a greater impact than expected.

There are three more limitations to our study that should be discussed. First, all analyses relied on empirical case data, which might be subject to the underascertainment bias. To minimize its impact on the estimated reproduction numbers, the reporting rate was assumed to be consistent throughout time, however, it may not hold for the entire course of the current epidemic. Asymptomatic instances were also reported through the contact tracing; however, these cases were excluded from the analysis because of the uncertainty regarding the detection rate. Second, regardless of the reproduction number, we set a constant value for the overdispersion parameter ($k = 0.1$) because this assumption ensures that the coefficient of variation of the negative binomial distribution is conserved; however, we have scarce data on how the variation in the offspring distribution of COVID-19 might change for different reproduction numbers. Third, we assumed that a mixture of two geometric distributions might adequately resemble the negative binomial distribution. The geometric distribution was chosen because it can effectively represent the long tail of the negative binomial distribution, and the calculated KL divergence of < 0.01 suggests that our approximation was plausible.

In conclusion, we quantitatively demonstrated that a decrease of more than 50% in high-risk transmission could maintain the reproduction number of COVID-19 of less than one, allowing the epidemic to be kept under control for a prolonged length of time. Socioeconomic activities should be carefully resumed while adequate precautionary measures are put in high-risk transmission settings to suppress sustained transmissions. Compared to stringent countermeasures like lockdowns, our proposed exit strategy from restrictive guidelines, with the classification of high- and low-risk settings, allows socioeconomic activities to be resumed while minimizing the risk of a resurgence of the disease.

Chapter 2: Supplementary materials

Condition that the next generation matrix is positive-definite

The next-generation matrix K derived by Equation (19) has to be a positive-definite matrix to be interpreted as reflecting the real-world transmission dynamics. This condition is equivalent to:

$$\begin{aligned} 0 < k_{LH} &= ab(R_H - R_L) < R_H, \\ 0 < k_{HL} &= \frac{q}{1 - q} k_{LH} < R_L. \end{aligned} \tag{S1}$$

Given $0 < a < 1$, $0 < q < 1$ and $q \neq 1 - a$, Equation (22) ensures $b < 0$ or $1 < b$. Therefore, k_{LH} and k_{LH} are both positive if and only if $b > 1$, which is equivalent to $q < 1 - a$. Under the condition $q < 1 - a$, $k_{LH} < R_H$ and $k_{HL} < R_L$ are equivalent to

$$\begin{aligned} q &< \frac{(1 - a)R}{aR_H + (1 - a)R}, \\ q &< \frac{(1 - a)R_L}{(1 - a)R_L + aR}, \end{aligned} \tag{S2}$$

both of which are smaller than $1 - a$, and thus the smaller of the two will be the upper bound of q. Their order of magnitude is identical to that between $\frac{\mu}{\lambda}$ and $\left(\frac{a}{1-a}\right)^2$. Ultimately, we get

$$\sup(q) = \begin{cases} \frac{(1 - a)R}{aR_H + (1-a)R} & \left(\frac{\mu}{\lambda} < \left(\frac{a}{1 - a}\right)^2\right), \\ \frac{(1 - a)R_L}{(1 - a)R_L + aR} & \left(\frac{\mu}{\lambda} > \left(\frac{a}{1 - a}\right)^2\right). \end{cases} \tag{S3}$$

In the present study, the estimated reproduction number for Period 1 (R_1) and the corresponding parameter values suggested $\frac{\mu}{\lambda} > \left(\frac{a}{1-a}\right)^2$ and that $\sup(q) < 0.015$. Therefore, we selected $q = 0.01$ for the baseline analysis.

Sensitivity analyses varying the overdispersion parameter and the relative size of the high-risk subgroup

Table S1 shows the estimated reproduction number under each scenario with varying values for the overdispersion parameter (*k)* of the negative binomial distribution and the high-risk proportion *q*. The upper and lower bounds of the CrI of *k* (i.e., 0.05 and 0.2) (Gilbert et al., 2020) and a smaller value of *q* of 0.001 were used for the sensitivity analysis. For $k = 0.05$, the baseline value $q = 0.01$ was not applicable because it did not yield a positive-definite next-generation matrix, therefore $q = 0.001$ was used instead.

Table S1. Estimated reproduction numbers of COVID-19 by scenario in Tokyo Metropolis and Osaka Prefecture by varying values of the overdispersion parameter (k) and the relative size of the high-risk subgroup (q)

Region	Scenario	k = 0.1 q = 0.01 (Baseline)	k = 0.1 q = 0.001	k = 0.05 q = 0.001	k = 0.2 q = 0.01
Including back-projected cases					
Tokyo Metropolis	'Back to normal'	1.78 (1.73–1.82)	1.78 (1.73–1.82)	1.78 (1.73–1.82)	1.78 (1.73–1.82)
	10% decrease	1.62 (1.58–1.66)	1.60 (1.56–1.64)	1.61 (1.57–1.64)	1.60 (1.56–1.64)
	30% decrease	1.30(1.27–1.33)	1.25 (1.22–1.28)	1.26 (1.23–1.29)	1.26 (1.23–1.29)
	50% decrease	0.98 (0.95–1.00)	0.90 (0.88–0.92)	0.93 (0.90–0.94)	0.92 (0.90–0.94)
Osaka Prefecture	'Back to normal'	1.58 (1.51–1.67)	1.58 (1.51–1.67)	1.58 (1.51–1.67)	1.58 (1.51–1.67)
	10% decrease	1.44 (1.38–1.49)	1.42 (1.36–1.48)	1.42 (1.37–1.48)	1.43 (1.37–1.48)
	30% decrease	1.16 (1.11–1.20)	1.11 (1.06–1.15)	1.12 (1.08–1.17)	1.12 (1.08–1.17)
	50% decrease	0.87 (0.84–0.90)	0.80 (0.77–0.83)	0.82 (0.78–0.85)	0.82 (0.79–0.85)
Including back-projected cases					
Tokyo Metropolis	'Back to normal'	1.74 (1.69–1.78)	1.74 (1.69–1.78)	1.74 (1.69–1.78)	1.74 (1.69–1.78)
	10% decrease	1.58 (1.54–1.62)	1.57 (1.53–1.60)	1.57 (1.53–1.61)	1.57 (1.53–1.61)
	30% decrease	1.27 (1.24–1.30)	1.22 (1.19–1.25)	1.23 (1.20–1.27)	1.23 (1.20–1.26)
	50% decrease	0.96 (0.93–0.98)	0.88 (0.86–0.90)	0.90 (0.88–0.92)	0.90 (0.88–0.92)
Osaka Prefecture	'Back to normal'	1.59 (1.52–1.65)	1.59 (1.52–1.65)	1.59 (1.52–1.65)	1.59 (1.52–1.65)
	10% decrease	1.45 (1.38–1.50)	1.43 (1.37–1.49)	1.43 (1.37–1.49)	1.43 (1.37–1.49)
	30% decrease	1.16 (1.11–1.21)	1.12 (1.07–1.16)	1.13 (1.08–1.17)	1.13 (1.08–1.17)
	50% decrease	0.88 (0.84–0.91)	0.80 (0.77–0.84)	0.82 (0.79–0.86)	0.82 (0.79–0.86)

Upper and lower 95% credible intervals obtained from the MCMC samples are shown in parentheses.

Sensitivity analysis varying the relative size of the high-risk subgroup

Table S2. Estimated next-generation matrices of COVID-19 in Tokyo Metropolis and Osaka Prefecture assuming the relative size of the high-risk subgroup (q) is 0.001

Region	Period 1*		Period 2		Period 3	
Including back-projected cases						
Tokyo Metropolis	k_{LL} = 0.08 (0.07–0.08)	k_{LH} = 5.90 (5.78–6.01)	k_{LL} = 0.05 (0.05–0.06)	k_{LH} = 2.96 (2.86–3.07)	k_{LL} = 0.05 (0.05–0.05)	k_{LH} = 2.59 (2.52–2.66)
	k_{HL} = 0.01 (0.01–0.01)	k_{HH} = 1.76 (1.71–1.80)	k_{HL} = 0.00 (0.00–0.00)	k_{HH} = 0.73 (0.70–0.76)	k_{HL} = 0.00 (0.00–0.00)	k_{HH} = 0.62 (0.60–0.64)
	R_1 = 1.78 (1.73–1.82)		R_2 = 0.74 (0.71–0.78)		R_3 = 0.63 (0.61–0.65)	
Osaka Prefecture	k_{LL} = 0.07 (0.07–0.07)	k_{LH} = 5.37 (5.19–5.54)	k_{LL} = 0.07 (0.06–0.07)	k_{LH} = 4.33 (4.19–4.47)	k_{LL} = 0.05 (0.04–0.05)	k_{LH} = 2.08 (1.95–2.20)
	k_{HL} = 0.01 (0.01–0.01)	k_{HH} = 1.56 (1.49–1.62)	k_{HL} = 0.00 (0.00–0.00)	k_{HH} = 1.18 (1.14–1.23)	k_{HL} = 0.00 (0.00–0.00)	k_{HH} = 0.47 (0.43–0.50)
	R_1 = 1.58 (1.51–1.64)		R_2 = 1.20 (1.15–1.25)		R_3 = 0.48 (0.44–0.51)	
Excluding cases with an unknown illness onset date						
Tokyo Metropolis	k_{LL} = 0.08 (0.07–0.08)	k_{LH} = 5.80 (5.68–5.90)	k_{LL} = 0.05 (0.05–0.05)	k_{LH} = 2.82 (2.71–2.93)	k_{LL} = 0.05 (0.05–0.05)	k_{LH} = 2.74 (2.66–2.81)
	k_{HL} = 0.01 (0.01–0.01)	k_{HH} = 1.72 (1.67–1.76)	k_{HL} = 0.00 (0.00–0.00)	k_{HH} = 0.69 (0.65–0.72)	k_{HL} = 0.00 (0.00–0.00)	k_{HH} = 0.66 (0.64–0.68)
	R_1 = 1.74 (1.69–1.78)		R_2 = 0.70 (0.67–0.73)		R_3 = 0.67 (0.65–0.70)	
Osaka Prefecture	k_{LL} = 0.07 (0.07–0.07)	k_{LH} = 5.40 (5.21–5.57)	k_{LL} = 0.06 (0.06–0.06)	k_{LH} = 4.06 (3.92–4.20)	k_{LL} = 0.05 (0.05–0.05)	k_{LH} = 2.25 (2.12–2.37)
	k_{HL} = 0.01 (0.01–0.01)	k_{HH} = 1.57 (1.50–1.63)	k_{HL} = 0.00 (0.00–0.00)	k_{HH} = 1.09 (1.04–1.14)	k_{HL} = 0.00 (0.00–0.00)	k_{HH} = 0.52 (0.48–0.55)
	R_1 = 1.59 (1.52–1.65)		R_2 = 1.10 (1.06–1.15)		R_3 = 0.53 (0.49–0.56)	

The values of k_{ij} describe the transmission rates from group j to group i, and R_n is the reproduction number in Period n derived from the estimated next-generation matrix. Upper and lower 95% credible intervals obtained from the MCMC samples are shown in parentheses.

*Three time periods were (1) the early invasion period (before 26 March 2020 for Tokyo and before 18 March 2020 for Osaka), (2) the period after an alert was declared by the prefectural governor of each region (26 March–7 April 2020 for Tokyo and 19 March–7 April 2020 for Osaka) and (3) the period after the governmental declaration of a state of emergency (8 April–25 May 2020 for Tokyo and 8 April–21 May 2020 for Osaka).

Sensitivity analysis varying the overdispersion parameter in the negative binomial distribution

Table S3. Estimated next-generation matrices of COVID-19 in Tokyo Metropolis and Osaka Prefecture assuming the overdispersion parameter (*k*) is 0.05 and the relative size of the high-risk subgroup (*q*) is 0.001

Region	Period 1 *		Period 2		Period 3	
Including back-projected cases						
Tokyo Metropolis	k_{LL} = 0.03 (0.03–0.03)	k_{LH} = 10.67 (10.46–10.87)	k_{LL} = 0.03 (0.03–0.03)	k_{LH} = 5.40 (5.22–5.59)	k_{LL} = 0.03 (0.03–0.03)	k_{LH} = 4.74 (4.61–4.86)
	k_{HL} = 0.01 (0.01–0.01)	k_{HH} = 1.71 (1.67–1.75)	k_{HL} = 0.01 (0.01–0.01)	k_{HH} = 0.70 (0.67–0.74)	k_{HL} = 0.00 (0.00–0.00)	k_{HH} = 0.60 (0.57–0.61)
	R_1 = 1.78 (1.73–1.82)		R_2 = 0.74 (0.71–0.78)		R_3 = 0.63 (0.61–0.65)	
Osaka Prefecture	k_{LL} = 0.03 (0.03–0.03)	k_{LH} = 9.72 (9.40–10.02)	k_{LL} = 0.03 (0.03–0.03)	k_{LH} = 7.85 (7.60–8.09)	k_{LL} = 0.03 (0.02–0.03)	k_{LH} = 3.83 (3.59–4.04)
	k_{HL} = 0.01 (0.01–0.01)	k_{HH} = 1.51 (1.45–1.58)	k_{HL} = 0.01 (0.01–0.01)	k_{HH} = 1.15 (1.10–1.19)	k_{HL} = 0.00 (0.00–0.00)	k_{HH} = 0.45 (0.41–0.48)
	R_1 = 1.58 (1.51–1.64)		R_2 = 1.20 (1.15–1.25)		R_3 = 0.48 (0.44–0.51)	
Excluding cases with an unknown illness onset date						
Tokyo Metropolis	k_{LL} = 0.03 (0.03–0.03)	k_{LH} = 10.48 (10.28–10.69)	k_{LL} = 0.03 (0.03–0.03)	k_{LH} = 5.15 (4.95–5.34)	k_{LL} = 0.03 (0.03–0.03)	k_{LH} = 5.00 (4.86–5.12)
	k_{HL} = 0.01 (0.01–0.01)	k_{HH} = 1.67 (1.63–1.71)	k_{HL} = 0.01 (0.01–0.01)	k_{HH} = 0.66 (0.63–0.69)	k_{HL} = 0.01 (0.00–0.01)	k_{HH} = 0.64 (0.61–0.66)
	R_1 = 1.74 (1.69–1.78)		R_2 = 0.70 (0.67–0.73)		R_3 = 0.67 (0.65–0.70)	
Osaka Prefecture	k_{LL} = 0.03 (0.03–0.03)	k_{LH} = 9.76 (9.44–10.08)	k_{LL} = 0.03 (0.03–0.03)	k_{LH} = 7.36 (7.12–7.62)	k_{LL} = 0.03 (0.02–0.03)	k_{LH} = 4.13 (3.90–4.35)
	k_{HL} = 0.01 (0.01–0.01)	k_{HH} = 1.52 (1.46–1.59)	k_{HL} = 0.01 (0.01–0.01)	k_{HH} = 1.05 (1.01–1.10)	k_{HL} = 0.00 (0.00–0.00)	k_{HH} = 0.50 (0.46–0.53)
	R_1 = 1.59 (1.52–1.65)		R_2 = 1.10 (1.06–1.15)		R_3 = 0.53 (0.49–0.56)	

The values of k_{ij} describe the transmission rates from group j to group i, and R_n is the reproduction number in Period n derived from the estimated next-generation matrix. Upper and lower 95% credible intervals obtained from the MCMC samples are shown in parentheses.

*Three time periods were (1) the early invasion period (before 26 March 2020 for Tokyo and before 18 March 2020 for Osaka), (2) the period after an alert was declared by the prefectural governor of each region (26 March–7 April 2020 for Tokyo and 19 March–7 April 2020 for Osaka) and (3) the period after the governmental declaration of a state of emergency (8 April–25 May 2020 for Tokyo and 8 April–21 May 2020 for Osaka).

Table S4. Estimated next-generation matrices of COVID-19 in Tokyo Metropolis and Osaka Prefecture assuming the overdispersion parameter (*k*) is 0.2 and the relative size of the high-risk subgroup (*q*) is 0.01

Region	Period 1 *		Period 2		Period 3	
Including back-projected cases						
Tokyo Metropolis	k_{LL} = 0.11 (0.11–0.12)	k_{LH} = 3.14 (3.08–3.20)	k_{LL} = 0.08 (0.07–0.08)	k_{LH} = 1.55 (1.50–1.61)	k_{LL} = 0.07 (0.07–0.07)	k_{LH} = 1.35 (1.31–1.39)
	k_{HL} = 0.03 (0.03–0.03)	k_{HH} = 1.72 (1.67–1.76)	k_{HL} = 0.02 (0.02–0.02)	k_{HH} = 0.71 (0.67–0.74)	k_{HL} = 0.01 (0.01–0.01)	k_{HH} = 0.60 (0.58–0.62)
	R_1 = 1.78 (1.73–1.82)		R_2 = 0.74 (0.71–0.78)		R_3 = 0.63 (0.61–0.65)	
Osaka Prefecture	k_{LL} = 0.11 (0.11–0.11)	k_{LH} = 2.86 (2.76–2.95)	k_{LL} = 0.10 (0.09–0.10)	k_{LH} = 2.29 (2.22–2.37)	k_{LL} = 0.06 (0.06–0.06)	k_{LH} = 1.08 (1.00–1.14)
	k_{HL} = 0.03 (0.03–0.03)	k_{HH} = 1.51 (1.46–1.58)	k_{HL} = 0.02 (0.02–0.02)	k_{HH} = 1.15 (1.10–1.20)	k_{HL} = 0.01 (0.01–0.01)	k_{HH} = 0.45 (0.42–0.49)
	R_1 = 1.58 (1.51–1.64)		R_2 = 1.20 (1.15–1.25)		R_3 = 0.48 (0.44–0.51)	
Excluding cases with an unknown illness onset date						
Tokyo Metropolis	k_{LL} = 0.11 (0.11–0.12)	k_{LH} = 3.09 (3.03–3.15)	k_{LL} = 0.07 (0.07–0.08)	k_{LH} = 1.48 (1.42–1.53)	k_{LL} = 0.07 (0.07–0.07)	k_{LH} = 1.43 (1.39–1.47)
	k_{HL} = 0.03 (0.03–0.03)	k_{HH} = 1.68 (1.64–1.72)	k_{HL} = 0.01 (0.01–0.02)	k_{HH} = 0.66 (0.63–0.70)	k_{HL} = 0.01 (0.01–0.01)	k_{HH} = 0.64 (0.62–0.66)
	R_1 = 1.74 (1.69–1.78)		R_2 = 0.70 (0.67–0.73)		R_3 = 0.67 (0.65–0.70)	
Osaka Prefecture	k_{LL} = 0.11 (0.11–0.11)	k_{LH} = 2.87 (2.77–2.96)	k_{LL} = 0.09 (0.09–0.09)	k_{LH} = 2.15 (2.07–2.77)	k_{LL} = 0.06 (0.06–0.07)	k_{LH} = 1.17 (1.10–1.23)
	k_{HL} = 0.03 (0.03–0.03)	k_{HH} = 1.54 (1.46–1.59)	k_{HL} = 0.02 (0.02–0.02)	k_{HH} = 1.06 (1.01–1.11)	k_{HL} = 0.01 (0.01–0.01)	k_{HH} = 0.50 (0.46–0.53)
	R_1 = 1.59 (1.52–1.65)		R_2 = 1.10 (1.06–1.15)		R_3 = 0.53 (0.49–0.56)	

The values of k_{ij} describe the transmission rates from group *j* to group *i*, and R_n is the reproduction number in Period *n* derived from the estimated next-generation matrix. Upper and lower 95% credible intervals obtained from the MCMC samples are shown in parentheses.

*Three time periods were (1) the early invasion period (before 26 March 2020 for Tokyo and before 18 March 2020 for Osaka), (2) the period after an alert was declared by the prefectural governor of each region (26 March–7 April 2020 for Tokyo and 19 March–7 April 2020 for Osaka) and (3) the period after the governmental declaration of a state of emergency (8 April–25 May 2020 for Tokyo and 8 April–21 May 2020 for Osaka).

Chapter 2 was originally published as:

Jung S-m, Endo A, Kinoshita R, Nishiura H. Projecting a second wave of COVID-19 in Japan with variable interventions in high-risk settings. *R. Soc. Open Sci*. 2021;8(3),202169. Minor formatting modifications and edits have been made for the dissertation.

Chapter 3: Predicting the effective reproduction number of COVID-19: inference using human mobility, temperature, and risk awareness

Background

Since the first confirmed case of SARS-CoV-2 infection was reported in Japan, the COVID-19 has continuously affected the entire country with the high infection rate of the disease and the existence of cases with no or mild symptoms. A surge of cases in early March led the Tokyo governor to issue a "stay-at-home" request on March 25, and the national government declared a state of emergency on April 16. In both cases, the government requested voluntary limitation of non-household contacts, and general public compliance with these interventions helped to suppress the surge of cases by June (Jung et al., 2021; Oshitani, 2020). However, after resuming socioeconomic activities in late May, the daily number of reported cases resurged exceeding the peak of daily reported cases observed during the "first wave" of the COVID-19 epidemic. Although a temporary decline in the incidence was observed, the country has experienced the third wave from late October. In response, prefectural governments with a large number of cases have requested bars and restaurants to curtail their operation hours from late November (e.g., asking their business to close by 9 pm) (Ministry of Health Labour and Welfare, 2020d). Despite these containment efforts, the spread of disease continued, leading the national government to declare the second state of emergency on 7 January 2021, asking citizens to refrain from non-essential outings (Cabinet Relations Office, 2021).

As part of an evaluation of countermeasures, the effective reproduction number (R_t), defined as the expected number of secondary cases arising from a single primary case at calendar time t, is widely used for monitoring the trend in the community-level transmissions (Nishiura et al., 2009). When the value of R_t is larger than one, an upward trend in incidence is likely, while the value below one suggests the opposite. Public health interventions should therefore aim to bring the R_t below one. Changes in the R_t should be routinely monitored to optimize the effectiveness of control measures (Thompson et al., 2019a). However, timely and accurate estimation of R_t using incidence data remains challenging. First, to precisely link the timing of a control measure and resulting changes in the transmission trend, it is vital to estimate the R_t as a function of the infection time (Gostic et al., 2020). Infection times are rarely observed in practice (only available

when the infector and time of infection are confirmed through the epidemiological investigation), thus, they need to be statistically estimated accounting for the empirical delay distributions (e.g., by the so-called "back-calculation" method). Moreover, the estimation of R_t is further complicated because of the right truncation with respect to the time interval from the infection to reporting. In real-time practice, the number of recent infections is underestimated due to cases that are already contracted to disease but not yet reported in the surveillance system. Considering the empirically observed time delay of around 9 days from the infection to reporting in Japan, the estimated R_t based on the reported incidence is likely to be biased, at least within 9 days from the latest reporting date.

Given that human-to-human contact facilitates SARS-CoV-2 transmission, digital proxies of human mobility patterns can provide an important avenue to infer the directly unobservable transmission patterns as a function of time. Indeed, multiple datasets of mobility patterns have widely available during the ongoing COVID-19 pandemic, and such datasets have been utilized to monitor the time-dependent patterns of the physical distancing performance (Buckee et al., 2020; Kishore et al., 2020; Leung et al., 2021; Nouvellet et al., 2021; Xiong et al., 2020). In addition, it has been suggested that higher transmissibility of COVID-19 is likely to be seen in low-temperature environments. (Li et al., 2020a; Pequeno et al., 2020; Qi et al., 2020; Smith et al., 2021; Ujiie et al., 2020; Wang et al., 2021). These data are often more readily accessible than case counts (which are typically subject to delays of ~9 days) and thus may enable near real-time assessment of interventions if they can be used to predict R_t. Furthermore, quantified degrees of risk awareness over COVID-19 can also help to predict R_t because the public awareness, inducing an adherence to personal protective behaviors (e.g., wearing a mask or washing hands with soap or sanitizers), may reduce the virus transmissions (West et al., 2020).

Accumulated evidence suggests that integrating human mobility coupled with temperature and risk awareness could well reflect the contact pattern as a function of time. Here, we aim to develop a simple statistical framework to predict the proxy of R_t using timely accessible data of these driving factors of SARS-CoV-2 transmissions (i.e., human mobility pattern, temperature, and risk awareness), which can provide an opportunity to infer the unobservable transmission patterns ahead of the formal empirical estimates subject to delays.

Methods

Epidemiological data

We retrieved the information of confirmed cases of COVID-19 in six prefectures in Japan: Tokyo, Osaka, Aichi, Hokkaido, Fukuoka, and Okinawa, from a publicly available data source, from 16 January 2020 through 15 February 2021 (Ministry of Health Labour and Welfare, 2020b). The data of six prefectures were categorized into two types: "training data" and "test data". The training data was used for the model training and cross-validation, while the test data was from regions not included in the training data and was used to evaluate the predictive performance of a trained model in different geographical settings. To ensure a sufficient number of cases is included in the training data, four prefectures (Tokyo, Osaka, Aichi, and Hokkaido) accounting for more than 200 cases before the first state of emergency were selected for the training data. The test data comprises two other prefectures (Fukuoka and Okinawa), which are geographically apart from those in the training data. According to the history of traveling abroad within 7 days prior to the illness onset, all cases were classified either as imported or domestic. A total of 217,258 confirmed COVID-19 cases including 166 imported cases were included in the study. Within the training data, 32,130 and 150,706 cases were assigned to the period for model training ("training period") and cross-validation ("validation period"), respectively, and 22,379 cases were included in the test data.

Reconstruction of COVID-19 incidence by the infection time

Of the 217,258 total cases, there were 114,277 (53%) confirmed COVID-19 cases with unknown illness onset dates. To estimate R_t as a function of the infection time, the back-projection was conducted following two steps. First, the missing illness onset date of those cases was back-projected from the date of laboratory confirmation with a right-truncated time interval distribution from illness onset to laboratory confirmation in each prefecture (Jung et al., 2021). Second, we back-projected the infection time among all reported COVID-19 cases from either observed or back-projected illness onset date, using the incubation period distribution (Linton et al., 2021). The *R* package "*surveillance*" (Höhle, 2007) was used for nonparametric back-projection.

Explanatory variable data

The human mobility pattern and temperature were hypothesized as driving factors for COVID-19 transmission, and those datasets for the abovementioned time period were collected. Google community mobility reports (hereafter Google mobility) were used to capture the human mobility patterns (Google, 2021). Google mobility data provides six different categories (i.e., "retail and recreation", "grocery and pharmacy", "parks", "transit stations", "workplaces", and "residential") of changes in the human mobility, relative to the average of that on the same day of the week in the pre-pandemic period (i.e., 3 January–6 February 2020). We used mobility patterns related to "retail and recreation" in our analyses based on our domain knowledge that this category likely represents the mobility in close-contact settings associated with COVID-19 transmissions (Cazelles et al., 2021). Daily temperature data were retrieved from Japan Meteorological Agency (Japan Meteorological Agency, 2021). Since daily temperature data is recorded at over 1,300 weather observatory stations, one representative observatory nearby the location of the prefectural government office was selected for each prefecture. In order to extract the overall trend of those time series without being influenced by daily noise, both datasets were smoothed by taking a 7-day moving average.

Model and statistical analysis

A prediction model for R_t, integrating the human mobility, temperature, and risk awareness, was designed and evaluated in the following steps. First, three candidate regression models were fitted to the reconstructed COVID-19 incidences during the training period via the renewal process. We then compared the performance of these candidate models by cross-validation against the estimated R_t from data in the validation period and selected the best model. Lastly, the predictive performance of the best-ranked model was evaluated using the separate test data by comparing estimated R_t with the predicted values produced by the trained model to determine the applicability of the model to other geographic settings.

Model for predicting the effective reproduction number

We propose three simple regression models that incorporate different combinations of explanatory factors for COVID-19 transmission: only Google mobility (Model 1), Google

mobility and temperature (Model 2), and Google mobility, temperature, and risk awareness over COVID-19 (Model 3). In each model, corresponding variables were included in a log-linear regression form. The R_t in the model with all three factors (Model 3) is formulated as follows:

$$R_{t,i} = R_{0,i} \exp\left(am_i(t) + bk_i(t) + c\min\left(w_{limit,i}, w_i(t)\right)\right), \quad (24)$$

where $R_{0,i}$ is the baseline effective reproduction number in prefecture i. We assume that $R_{0,i}$ are similar between all four prefectures of the training data, and follow the Gamma distribution with a mean $\bar{R}$ and fixed coefficient of variation (CV) of 0.5 (Park et al., 2020). We fixed the value of CV due to a small number of prefectures, but varied CV in the range of 0.25–1 carried similar results of our analysis. Covariates $m_i(t)$ and $k_i(t)$ are smoothed values of Google mobility and temperature at calendar time t and in prefecture i, respectively. $w_i(t)$ is the degree of risk awareness at calendar time t and in prefecture i, which was graded by assuming that it is linearly associated with the smoothed number of newly reported COVID-19 cases, following a positive association between the confirmed cases and risk perception from the study using a longitudinal data in the UK (Schneider et al., 2021). The effect of this variable $w_i(t)$ was capped at a predefined upper limit ($w_{limit,i}$), corresponding to the governmental definition of the "highest alert level" incidence in Japan (i.e., 25 confirmed cases per 100,000 population in a week) (Cabinet Relations Office, 2020). According to the definition, a daily number of cases giving an upper limit for each prefecture i ($w_{limit,i}$) was specified as 497 in Tokyo, 315 in Osaka, 270 in Aichi, 188 in Hokkaido, 182 in Fukuoka, and 52 in Okinawa. The R_t in Models 1 and 2 were specified as models whose coefficients for non-included variables in Equation (24) were fixed at 0.

We constructed a likelihood function for the proposed regression models of R_t (Model 1–3), based on the renewal process and estimated the corresponding parameters of each regression model by fitting it to the COVID-19 incidence during the training period. The expected number of daily reported domestic cases $c_{domestic,i}(t)$ at calendar time t in a given prefecture i was calculated using the equation:

$$\mathrm{E}\left(c_{domestic,i}(t)\right) = R_{t,i} \sum_{\tau=1}^{t-1} c_{total,i}(t-\tau) g(\tau) \frac{F_i(T-t)}{F_i(T-t+\tau)}, \quad (25)$$

where $c_{total,i}(t)$ denotes the daily number of COVID-19 cases at time t reported in prefecture i (including both imported and domestic cases). $g(\cdot)$ is the probability mass function of generation time (Nishiura et al., 2020d). To account for the right truncation, the cumulative mass function, $F_i(\cdot)$, for the time delay from infection to report was calculated by convoluting the probability mass function of the incubation period and of the time interval from illness onset to reporting in prefecture i. The used training period covered the first pandemic wave in Japan (15 March–1 May 2020) and a part of the second wave (15 July–31 August 2020). The intra-wave period from 1 May to 15 July 2020 was excluded because of low count numbers observed during that period. For parameter estimation, Poisson likelihood was used:

$$\mathrm{L}\left(\theta; c_{domestic,i}(t)\right) = \prod_{t=1}^{T} \frac{\exp\left(-E\left(c_{domestic,i}(t)\right)\right)\left(E\left(c_{domestic,i}(t)\right)\right)^{c_{domestic,i}(t)}}{c_{domestic,i}(t)!}, \quad (26)$$

where the set θ includes all or a part of the parameters (i.e., $R_{0,i}$, $\bar{R}$, a, b, and c) specific for each of the three proposed models. The maximum likelihood method was employed, 95% confidence intervals (CIs) of each parameter were derived from 10,000 samples from a Laplace-approximate normal distribution.

Model selection through cross-validation

To select the best model among proposed models, cross-validation was conducted by comparing the predicted and estimated "ground-truth" R_t during the validation period (from 1 September 2020 to 31 January 2021) in the four prefectures. Each regression model produced predictive R_t values for the validation period using the explanatory variables based on the estimated parameters. We used the R_t values estimated from incidence data via the renewal process (Equation 25) as the ground-truth. R_t was estimated as a free time-dependent parameter from the COVID-19 incidences during the validation period by the following likelihood function:

$$\mathrm{L}\left(R_{t,i}; c_{domestic,i}(t)\right) = \prod_{t=1}^{T} \frac{\exp\left(-E\left(c_{domestic,i}(t)\right)\right)\left(E\left(c_{domestic,i}(t)\right)\right)^{c_{domestic,i}(t)}}{c_{domestic,i}(t)!}. \quad (27)$$

The 95% CIs were derived using the profile likelihood method. Considering the right-truncation in the recently reported incidences, the estimated R_t for the latest 15 days (1–15 February 2020) were excluded from the cross-validation. Furthermore, to smooth out abrupt fluctuations (e.g.,

superspreading events) in the estimated R_t values, a 7-day moving average was taken. Then, the predictive performance of each model (i.e., comparison between the predicted and estimated R_t during the validation period) was quantitatively assessed using four different measurements: bias, root-mean-square error (RMSE), ranked probability score, and Dawid-Sebastiani score (Funk et al., 2019), and the best model was selected. In addition, the number of predicted infections using the conditional forecasting method (i.e., forecasting a future incidence based on the predicted R_t and empirically reported incidences in the past) was also compared against the back-projected incidence by infection dates.

Evaluation of the predictive performance using the test data

Lastly, the predictive performance of the finally selected model was evaluated using the test data, indicating the potential applicability of the proposed model to other geographical settings. Accordingly, the R_t values in two prefectures of test data (Fukuoka and Okinawa) were predicted from 15 July 2020 through 31 January 2021, relying only on the trained model, and were compared against the estimated R_t from the renewal process. In addition, the predicted number of infections using the conditional forecasting method was also compared with the empirical data in each of the two prefectures.

Results

Figure 6 shows the epidemic curve of COVID-19 by reporting date in four selected prefectures in the training data, along with the time trend of Google mobility and temperature. Following a substantial reduction in Google mobility across all regions, the number of reported COVID-19 cases also decreased. On consecutive national holidays, human mobility patterns tended to show abrupt increases, and the number of reported cases increased slightly after roughly 9 days, consistent with the empirical time delay from infection to reporting in Japan.

Table 3 shows the estimated parameters from the data in the training period and summarizes the predictive performance of proposed models during the validation period. Based on the Dawid-Sebastiani score, the model that incorporated Google mobility, temperature, and risk awareness (Model 3) was selected as the best model, while the model that only accounted for Google mobility (Model 1) showed the best performance in RMSE, bias, and ranked probability score.

However, when compared to Model 3, the predicted time trend of R_t using Model 1 (almost linear trend near the value of one; Figure S1) was less informative, indicating that Model 1 could be not suitable for the time trend analysis. As a result, Model 3 was chosen as the best model. Using Model 3, the estimated baseline value $R_{0,i}$ was estimated at 4.40 (95% CI: 4.07–4.73) for Tokyo, 2.85 (95% CI: 2.62–3.07) for Osaka, 2.20 (95% CI: 2.02–2.38) for Aichi, and 1.99 (95% CI: 1.84–2.15) for Hokkaido. The regression coefficient accounting for Google mobility was estimated to be 0.03 per percent point (95% CI: 0.03–0.03), while temperature and risk awareness were negatively associated with estimated coefficients of -0.02 per Celsius degree (95% CI: -0.02–-0.01) and -0.12 per 100 reported cases (95% CI: -0.15–-0.10), respectively. All coefficients were statistically significant.

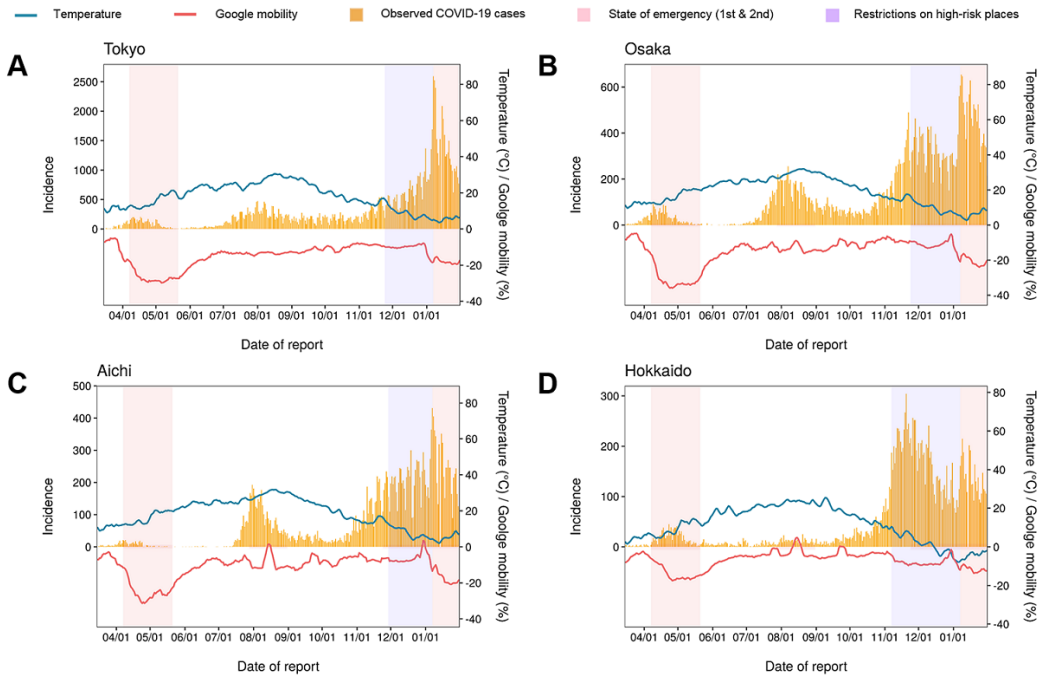

Figure 6. **Epidemiological curves of COVID-19 by date of report, along with the trend of Google mobility and temperature in Tokyo, Osaka, Aichi, and Hokkaido, Japan.**

The number of COVID-19 cases by date of report (yellow bars) from 15 Mar 2020–12 Jan 2021 in four prefectures of Japan in the training data: (A) Tokyo, (B) Osaka, (C) Aichi, and (D) Hokkaido. Red lines indicate trends of changes in human mobility patterns (i.e., "retail and recreation" category in Google community mobility reports) compared with that in the pre-pandemic period (i.e., 3 January–6 February 2020). Blue lines show trends of the daily temperature in each region and both mobility and temperature were smoothed using a 7-day moving average. In each figure, two red shaded areas indicate time periods for the nation-wide first and second state of emergency, respectively, while purple shaded areas show the time period when stringent restrictions on bars and restaurants were implemented by each prefectural government right before the second state of emergency.

Table 3. Summary of the estimated parameters and predictive performance of the proposed models

Model	Parameter	Value	Bias	RMSE	Ranked probability score	Dawid-Sebastiani score
Model 1	R_0 (Tokyo)	1.74 (1.66–1.82)	0.28	1.65	168.94	479,953
	R_0 (Osaka)	1.37 (1.32–1.41)				
	R_0 (Aichi)	1.15 (1.11–1.19)				
	R_0 (Hokkaido)	1.33 (1.25–1.41)				
	Google mobility	0.02 (0.01–0.02)				
Model 2	R_0 (Tokyo)	4.39 (4.05–4.72)	-1.06	2.29	264.41	328,849
	R_0 (Osaka)	3.23 (3.02–3.44)				
	R_0 (Aichi)	2.59 (2.43–2.75)				
	R_0 (Hokkaido)	2.09 (1.95–2.23)				
	Google mobility	0.03 (0.03–0.03)				
	Temperature	-0.03 (-0.03–-0.03)				
Model 3	R_0 (Tokyo)	4.40 (4.07–4.73)	0.55	1.77	171.60	147,027
	R_0 (Osaka)	2.85 (2.62–3.08)				
	R_0 (Aichi)	2.20 (2.02–2.38)				
	R_0 (Hokkaido)	1.99 (1.84–2.15)				
	Google mobility	0.03 (0.03–0.03)				
	Temperature	-0.02 (-0.02–-0.01)				
	Risk awareness	-0.12 (-0.15–-0.10)				

Model 1: Google mobility; Model 2: Google mobility and temperature; Model 3: Google mobility, temperature, and risk awareness; RMSE: root-mean-square-error.

Each value describes the estimated parameters of three different models and 95% confidence intervals derived by maximum likelihood estimation and Laplace-approximate normal distribution. Predictive performances of each model were compared using three measures (i.e., root-mean-square error, ranked probability score, and Dawid-Sebastiani score) and summing estimates of four regions of the training data.

Figure 7 shows the comparison of the estimated and predicted R_t for four prefectures of the training data using the best-ranked Model 3. Despite that the model was fitted to cases over a relatively short period of time, the predicted values and 95% CIs overall well captured the temporal patterns of the estimated R_t in all the prefectures, showing clear signs of R_t rising above 1 at the beginning of the second and third waves of the epidemic. However, with the implementation of stringent countermeasures (e.g., curtailing opening hours of night-life spots) from November 2020, the predicted R_t showed larger deviations from the estimated values, implying a deterioration in predictive performance. The predicted R_t using Model 1 (Figure S1) and Model 2 (Figure S2) were less consistent with the estimated R_t.

Figure 8 shows the test performance of the best model (Model 3), by comparing the estimated and predicted R_t in Fukuoka and Okinawa (test data). With the default value of $R_{0,i}$ offset to 2.50, the inferred R_t were consistent with the overall trend of the ground-truth R_t values, indicating the applicability of the proposed model to other geographical and climatological settings.

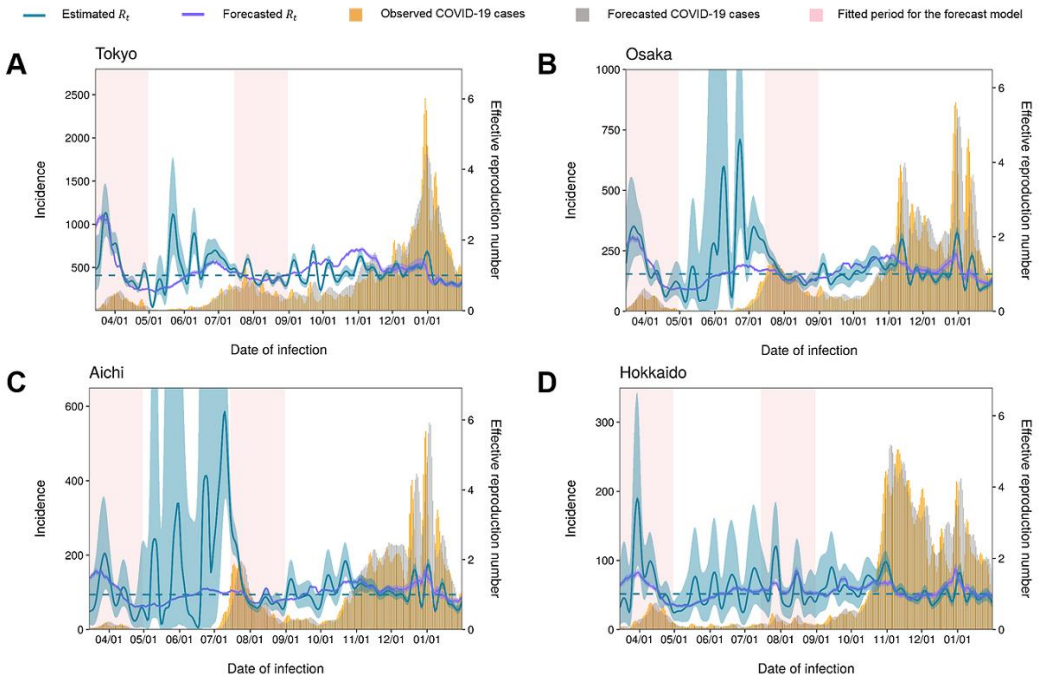

Figure 7. Comparison of the estimated and predicted effective reproduction number of COVID-19 using the model accounting for Google mobility, temperature, and risk awareness.

Comparison between the estimated and predicted effective reproduction number (R_t) of COVID-19. The model (considering Google mobility, temperature, and risk awareness on COVID-19; Model 3) was applied to four prefectures of Japan in the training data: (A) Tokyo, (B) Osaka, (C) Aichi, and (D) Hokkaido. Yellow bars represent reconstructed numbers of COVID-19 cases by infection time and grey bars show the number of predicted incidences using the conditional forecasting method. Blue lines and shaded areas indicate the estimated R_t and its 95% confidence intervals using the renewal process and profile likelihood, while purple lines and shaded areas are the predicted R_t and its 95% confidence interval derived from the Laplace-approximate normal distribution. Red shaded areas indicate the training period (i.e., 15 March–1 May 2020 and 15 July–31 August 2020) used for estimating parameters of the model.

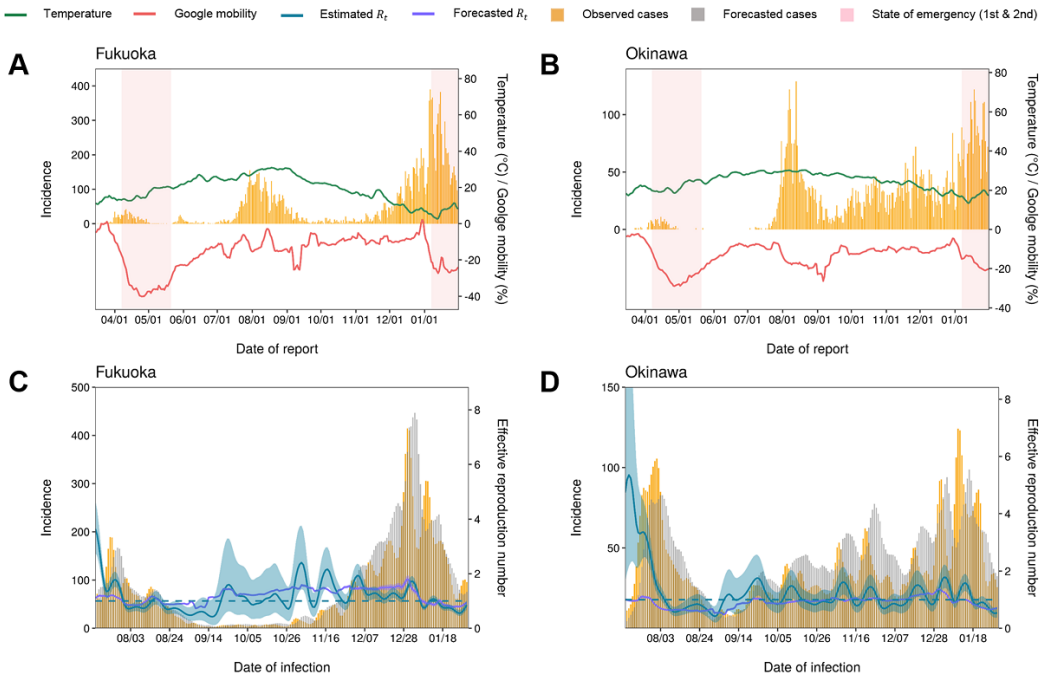

Figure 8. Comparison of the estimated and predicted effective reproduction number of COVID-19 using the best model and two other geographic settings (test data) in Japan.

(A–B) The number of COVID-19 cases by date of report (yellow bars) from 15 March 2020–12 January 2021 in two prefectures of the test data: (A) Fukuoka and (B) Okinawa. Red lines indicate trends of changes in human mobility patterns (i.e., the "retail and recreation" category in Google community mobility reports), and green lines show trends of the daily temperature in each region. Both mobility and temperature were smoothed using a 7-day moving average. (C–D) Comparison between the estimated and predicted effective reproduction number (R_t) of COVID-19 using the best model (considering Google mobility, temperature, and risk awareness; Model 3) and the test data: (C) Fukuoka and (D) Okinawa. Yellow bars represent reconstructed numbers of COVID-19 cases by infection time and grey bars show the number of predicted incidences using the conditional forecasting method. Blue lines and shaded areas indicate the estimated R_t and its 95% confidence intervals using the renewal process and profile likelihood, while purple lines and shaded areas are the predicted R_t and its 95% confidence interval from the best model and its estimated parameters.

Discussion

The present study has quantitatively shown that our proposed simple regression model can predict the R_t of COVID-19 in a real-time manner, accounting for human mobility, temperature, and risk awareness. In addition, our analysis suggested that the human mobility pattern was positively associated with COVID-19 transmissions, while the temperature and risk awareness were negatively associated.

The inverse association between the temperature and SARS-CoV-2 transmissions is consistent with other published papers (Li et al., 2020a; Ma et al., 2021; Smith et al., 2021). This finding could be explained by two possible mechanisms. First, cold temperature induces behavioral changes and increases indoor contact (i.e., close physical contact in poorly ventilated spaces), all of which are linked to elevation in the SARS-CoV-2 transmission risk (McClymont and Hu, 2021). Second, the virus enjoys greater survivability in cold environments (Riddell et al., 2020), as was the case for other human coronaviruses (Chan et al., 2011; van Doremalen et al., 2013). The number of reported cases during the summer season was higher than that of the winter season in 2020 (Figure 1), however, it should be approached with caution due to the mixture of multiple factors. As the initial population-wide restrictions were lifted at the start of the 2020 summer (i.e., 25 May 2020), the resumption of socioeconomic activities could result in a substantial increase in physical contact. In fact, the majority of SARS-CoV-2 infections reported in the early summer of 2020 were linked to nightspot-related clusters, which was thought to be the trigger of the following upsurge of incidence (Ministry of Health Labour and Welfare, 2020e).

Our findings also indicate that the reduction in socioeconomic activities and the level of risk awareness may be linked to the reduction in transmission, highlighting the potential of social distancing interventions and risk communication for controlling the COVID-19 epidemic (Anderson et al., 2020; Heydari et al., 2021). However, unlike our assumption that risk awareness is linearly related to the number of newly reported cases, the association between the number of COVID-19 cases and the degree of risk awareness may change over time in the long run. Despite that a positive correlation between the number of reported COVID-19 cases and people's risk awareness has been reported, risk awareness can be also influenced by

psychological factors, not only objective factors like case counts (Schneider et al., 2021). For instance, in spite of the continuously increasing number of reported COVID-19 cases, adherence to personal protective behaviors among residents might be reduced if they believe in such behaviors are not being able to make a significant difference in preventing the virus from spreading. Nevertheless, we believe that the model with risk awareness (Model 3) performs well enough in terms of the prediction of R_t to achieve the primary goal of the study, and it outperforms all other models (Model 1 & 2).

It is remarkable that the predicted R_t by a simple linear regression model fitted to the very limited data points well aligned with the estimates empirically obtained from the time series of COVID-19 incidence, showing a clear emerging signal (R_t>1) of the second and third waves in Japan. Such performance of the proposed model suggests that our framework can provide a plausible proxy of the latest R_t of COVID-19 using the readily accessible data, which conventional methods relying on the reported incidence are not able to provide in a timely manner due to the inherent delays. Timely assessment of R_t is essential to inform public health policy. Especially, it allows us to suppress the number of severe cases before the intensive care unit occupancy reaches full capacity, which is critical to secure the resilience of the healthcare system during the ongoing COVID-19 pandemic. The proposed model could not fully capture abrupt changes of R_t values, which were presumably caused by temporary local surges of cases (e.g., clusters in hospitals and nursing homes). However, it was still able to provide a timely signal of changes in R_t before the estimates from the conventional method (obtained from the case counts) become available.

Despite the overall good performance of the proposed model, our framework over- or underestimated the R_t when stringent interventions (i.e., reducing opening hours for restaurants and bars from November 2020 and implementation of the second state of emergency from 7 January 2021) were in place. Although our domain knowledge leads us to believe that the mobility patterns associated with retail and recreation can represent the physical mixing in high-risk settings, such mobility data with limited temporal and spatial resolution may not fully reflect the detailed social contact patterns. The transmission of COVID-19 is well known to involve substantial individual variations, as evidenced by an empirically observed highly dispersed offspring distribution (Endo et al., 2020; Nishiura et al., 2020c) and thus stringent control

measures were imposed primarily on settings regarded as high-risk (e.g., nightclubs, bars, and restaurants). The resulting changes in detailed contact patterns in those places may not have been fully reflected on the simple summary data of human mobility. Moreover, the digital proxies for human mobility patterns were suggested to be not very informative regarding changes in the density of individuals within high-risk places, although this metric may play a crucial role in the SARS-CoV-2 (Chang et al., 2021). These limitations of the mobility data may account for the temporary deviations in the prediction. The spatially and socially more precise analysis could be conducted in the future, once more detailed information on the physical mixing patterns (e.g., exact location within the building and density of visits) is available.

There are some additional limitations to be mentioned. First, the upper limit for the effect of risk awareness was rather arbitrary chosen and not necessarily theoretically justified. We assumed that risk awareness can reduce the transmission risk through personal behavioral changes that are not reflected in the changes in mobility (e.g., wearing a mask or avoiding crowded places during outside visits). However, there is likely to be a certain limit to the risk reduction achieved by such personal behavioral changes, thus, we have incorporated it in our model as a prespecified cap. Second, with the nationwide COVID-19 vaccine roll-out, the proposed model might become insufficient to predict the R_t due to the decrease in the proportion of susceptible in the population conferred by vaccination. Third, the emergence of new SARS-CoV-2 variants was not taken into account in our model. When a highly transmissible variant outcompetes the existing variants, the baseline effective reproduction number (R_0 in Equation (24)) should be adjusted according to the relative transmissibility of the corresponding variant. Lastly, additional heterogeneities (e.g., age-specific infectiousness and susceptibility) are not fully considered. An extended model that accounts for age-stratified transmission dynamics, as well as age-specific mobility patterns, may be required to conduct more accurate predictions.

In conclusion, the present study demonstrates that human mobility, temperature, and risk awareness can be integrated into the renewal process to timely predict the effective reproduction number, ahead of the formal empirical estimates subject to delays. The proposed model provides essential information for timely planning and assessment of control measures during the ongoing COVID-19 transmission.

Supplementary materials

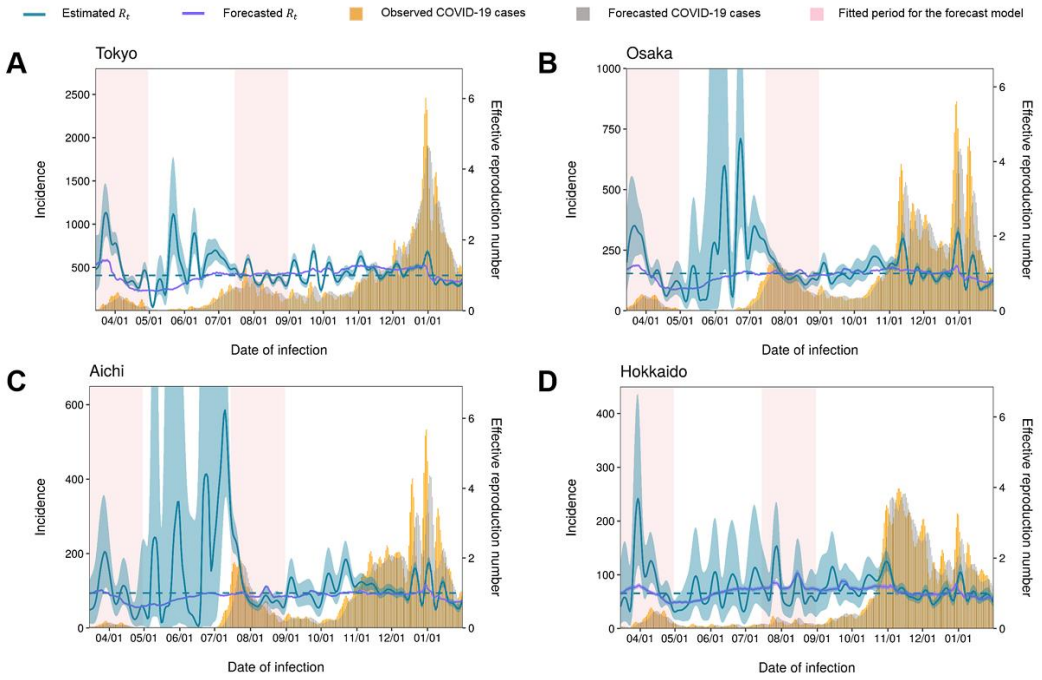

Figure S1. Comparison of estimated and predicted effective reproduction number of COVID-19 using the model incorporated with only Google mobility.

Comparison between the estimated and predicted effective reproduction number (R_t) of COVID-19 using the model (considering only Google mobility; Model 1) in four prefectures of Japan in the training data: (A) Tokyo, (B) Osaka, (C) Aichi, and (D) Hokkaido. Yellow bars represent reconstructed numbers of COVID-19 cases by infection time and grey bars show the number of predicted incidences using the conditional forecasting method. Blue lines and shaded areas indicate the estimated R_t and its 95% confidence intervals using the renewal process and profile likelihood, while purple lines and shaded areas are the predicted R_t and its 95% confidence interval derived from the Laplace-approximate normal distribution. Red shaded areas indicate the training period (i.e., 15 March–1 May 2020 and 15 July–31 August 2020) used for estimating parameters of the model.

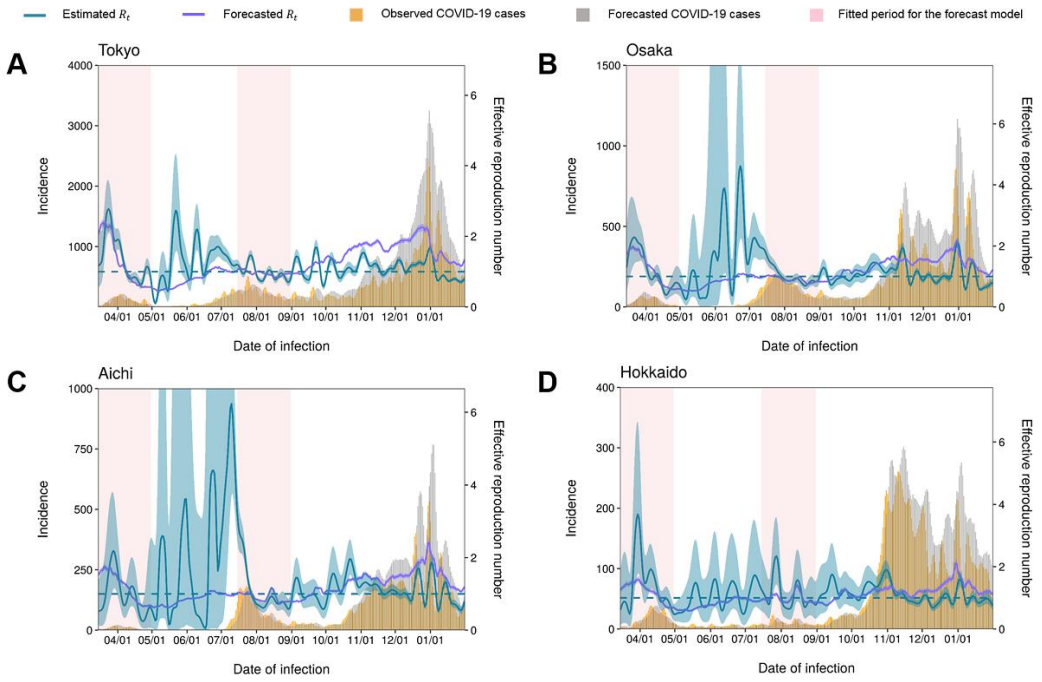

Figure S2. Comparison of estimated and predicted effective reproduction number of COVID-19 using the model incorporated with Google mobility and temperature.

Comparison between the estimated and predicted effective reproduction number (R_t) of COVID-19 using the model (considering Google mobility and temperature; Model 2) in four prefectures of Japan in the training data: (A) Tokyo, (B) Osaka, (C) Aichi, and (D) Hokkaido. Yellow bars represent reconstructed numbers of COVID-19 cases by infection time and grey bars show the number of predicted incidences using the conditional forecasting method. Blue lines and shaded areas indicate the estimated R_t and its 95% confidence intervals using the renewal process and profile likelihood, while purple lines and shaded areas are the predicted R_t and its 95% confidence interval derived from the Laplace-approximate normal distribution. Red shaded areas indicate the training period (i.e., 15 March–1 May 2020 and 15 July–31 August 2020) used for estimating parameters of the model.

Chapter 3 was originally published as:

Jung S-m, Endo A, Akhmetzhanov AR, Nishiura H. Predicting the effective reproduction number of COVID-19: inference using human mobility, temperature, and risk awareness. *Int J Infect Dis*. 2021;113:47-54. Minor formatting modifications and edits have been made for the dissertation.

Conclusion

With more than 5 million COVID-19 deaths (Johns Hopkins University, 2021), the COVID-19 pandemic has had considerable impacts on healthcare systems all around the world. In response, a variety of non-pharmaceutical interventions, which are seen as important tools in tackling the growing COVID-19 incidence, has been implemented in many of the most affected areas (Perra, 2021). However, such broad restrictions had also resulted in profound impacts on individuals and society (Bavel et al., 2020). Therefore, in order to develop a well-tailored response strategy to the COVID-19 pandemic, an in-depth understanding of its infection dynamics is necessary, and it should be guided by quantitative assessment based on the reconstructed infection dynamics.

Chapter 1 statistically estimated the severity and transmissibility of COVID-19 in the early stage of the pandemic using the exported cases data. Then, *Chapter 2* quantified the next-generation matrix accounting for the high- and low-risk transmissions settings and explored sustainable exit strategies by projecting a second wave of the COVID-19 epidemic in Japan with different levels of restriction. Lastly, *Chapter 3* suggested a statistical framework for providing the effective reproduction number of COVID-19 in a real-time manner, by integrating human mobility with temperature and risk awareness. Using a mathematical modelling approach and publicly available data, these three chapters of the dissertation provide the following insights into the infection dynamics of COVID-19.

- *Chapter 1*: Given the estimated confirmed case fatality risk and basic reproduction number of COVID-19, the substantial potential for causing a pandemic was identified in the very early stage of the pandemic, when only 20 exported cases were confirmed outside China. The proposed approach can help direct risk assessment in other settings with the use of the publicly available dataset. In addition, the estimated growth rate of the incidence in China was used for precise estimation of other epidemiological parameters (e.g., distribution of incubation period and time delay from onset to hospitalization) to take account for right-censored cases during the early stage of the pandemic (Linton et al., 2020).

- *Chapter 2*: The projected wave of COVID-19 in Japan suggested that implementing sufficient precautionary measures to suppress transmissions in high-risk settings could keep the epidemic under control while resuming socioeconomic activities. It implies that understanding the infection dynamics of COVID-19 with the classification of high- and low-risk transmission settings is essential in developing a more efficient and sustainable exit strategy. Indeed, such finding has been practically utilized in public health decision-making in Japan as a motive of "quasi-state of emergency" (i.e., imposing stringent interventions only in specific settings with a high-risk transmission).

- *Chapter 3*: The proposed framework integrated with human mobility, temperature, and risk awareness can provide a timely prediction of the effective reproduction number of COVID-19, which are not able to be provided by the conventional method relying on reported incidence due to the inherent delays. This framework can shed light on inferring directly unobserved transmission patterns as a function of time, and it has been used to inform public health policies for planning timely epidemic control measures in practice (Ministry of Health Labour and Welfare, 2021a).

Given the rapid spread of new SARS-CoV-2 variants with higher transmissibility (Ministry of Health Labour and Welfare, 2021b) and nationwide vaccine roll-out (Ministry of Health Labour and Welfare, 2021c), consideration of these impacts on the infection dynamics of COVID-19 should be done as a future study. Despite the remained tasks, the present dissertation with three chapters has provided a better knowledge of COVID-19 infection dynamics and shown practical applications to developing an evidence-based response strategy for minimizing the burden of the ongoing COVID-19 pandemic.

Acknowledgments

Throughout the writing of this dissertation, I have received a great deal of support and assistance.

First, I owe a deep sense of gratitude to my supervisor Hiroshi Nishiura whose insight and knowledge into the subject matter steered me throughout my Ph.D. course. Since I first met him in the 2016 Summer Boot Camp in Tokyo, he has been an ideal and the best supervisor, mentor, and running mate. He always provided me countless opportunities with full encouragement and enthusiasm. Especially, his tremendous energy and invaluable advice motivated me to navigate myself to pursue my future career as a researcher. I cannot express my gratitude and appreciation enough and without his guidance, this dissertation would not have been accomplished. An immense thank also to Tamakoshi Akiko and all members of my dissertation committee—Tatsuya Atsumi, Takanori Teshima, Satoshi Konno, Toshiyuki Nagai, Isao Yokota, and Kayo Ueda—for their support and insightful remarks on my dissertation.

I would like to especially thank Andrei Akhmetzhanov, Akira Endo, and Ryo Kinoshita for their stimulating questions and valuable comments on my Ph.D. work. Thanks to them, I could have lovely discussions which were vital in inspiring me to think logically. I am also thankful to all lab members (present and previous) and collaborators—including Robin Thompson, Fuminari Miura, Louis Yat Hin Chan, and Jaehun Jung—for so many lessons to learn.

Getting through my dissertation required more than academic support, and I have many, many people to thank for listening to and, at times, having to tolerate me over the past three years. I would like to thank all the administrative staff—Hisae Hirama, Miwako Inagi, Keiko Saito, and Ikumi Karakawa—for their kind supports. I would also like to thank my friends and Kinoshita family for helping me to quickly adjust to Japan and for many memorable days in Japan. I must express my very profound gratitude to my family and my partner Sayaka for providing me with unfailing support and continuous encouragement throughout my years of study and through the process of researching and writing this dissertation.

Lastly, I would like to thank the financial support from the Ministry of Education, Culture, Sports, Science and Technology (MEXT) Research Scholarship and the Japan Society for the Promotion of Science (JSPS) DC1 Research Fellowship (20J2135800).

Disclosure of conflicts of interest

Chapter 1: All authors declare no conflict of interest.

Chapter 2: Endo A. received research funding from Taisho Pharmaceutical Co., Ltd.

Chapter 3: Endo A. received research funding from Taisho Pharmaceutical Co., Ltd.

References

Anderson, R.M., Heesterbeek, H., Klinkenberg, D., and Hollingsworth, T.D. (2020). How will country-based mitigation measures influence the course of the COVID-19 epidemic? Lancet *395*, 931–934.

Bavel, J.J. Van, Baicker, K., Boggio, P.S., Capraro, V., Cichocka, A., Cikara, M., Crockett, M.J., Crum, A.J., Douglas, K.M., Druckman, J.N., et al. (2020). Using social and behavioural science to support COVID-19 pandemic response. Nat. Hum. Behav. *4*, 460–471.

BBC NEWS Coronavirus: Wuhan Shuts Public Transport over Outbreak.

Boldog, P., Tekeli, T., Vizi, Z., Dénes, A., Bartha, F.A., and Röst, G. (2020). Risk assessment of novel coronavirus COVID-19 outbreaks outside China. J. Clin. Med. *9*, 571.

Buckee, C.O., Balsari, S., Chan, J., Crosas, M., Dominici, F., Gasser, U., Grad, Y.H., Grenfell, B., Halloran, M.E., Kraemer, M.U.G., et al. (2020). Aggregated mobility data could help fight COVID-19. Science *368*, 145–146.

Cabinet Relations Office (2020). Advisory committee for COVID-19.

Cabinet Relations Office (2021). Ongoing Topics.

Cazelles, B., Comiskey, C., Nguyen-Van-Yen, B., Champagne, C., and Roche, B. (2021). Parallel trends in the transmission of SARS-CoV-2 and retail/recreation and public transport mobility during non-lockdown periods. Int. J. Infect. Dis. *104*, 693–695.

Center for Disease Control and Prevention (2020). 2019 Novel Coronavirus, Wuhan, China.

Chan, J.F.-W., Yuan, S., Kok, K.-H., To, K.K.-W., Chu, H., Yang, J., Xing, F., Liu, J., Yip, C.C.-Y., and Poon, R.W.-S. (2020). A familial cluster of pneumonia associated with the 2019 novel coronavirus indicating person-to-person transmission: a study of a family cluster. Lancet *395*, 514–523.

Chan, K.H., Peiris, J.S.M., Lam, S.Y., Poon, L.L.M., Yuen, K.Y., and Seto, W.H. (2011). The Effects of Temperature and Relative Humidity on the Viability of the SARS Coronavirus. Adv. Virol. *2011*, 734690.

Chang, S., Pierson, E., Koh, P.W., Gerardin, J., Redbird, B., Grusky, D., and Leskovec, J. (2021). Mobility network models of COVID-19 explain inequities and inform reopening. Nature *589*, 82–87.

Chinese National Health Commission (NHC) (2021). Experts answer reporters' questions on pneumonia outbreak of new coronavirus infection].

Cui, J., Li, F., and Shi, Z.-L. (2019). Origin and evolution of pathogenic coronaviruses. Nat. Rev. Microbiol. *17*, 181–192.

Donnelly, C.A., Ghani, A.C., Leung, G.M., Hedley, A.J., Fraser, C., Riley, S., Abu-Raddad, L.J., Ho, L.-M., Thach, T.-Q., and Chau, P. (2003). Epidemiological determinants of spread of causal agent of severe acute respiratory syndrome in Hong Kong. Lancet *361*, 1761–1766.

van Doremalen, N., Bushmaker, T., and Munster, V.J. (2013). Stability of Middle East respiratory syndrome coronavirus (MERS-CoV) under different environmental conditions. Euro Surveill. *18*.

Endo, A., Abbott, S., Kucharski, A.J., and Funk, S. (2020). Estimating the overdispersion in COVID-19 transmission using outbreak sizes outside China. Wellcome Open Res. *5*, 67.

Fraser, C., Riley, S., Anderson, R.M., and Ferguson, N.M. (2004). Factors that make an infectious disease outbreak controllable. Proc. Natl. Acad. Sci. U. S. A. *101*, 6146 LP – 6151.

Funk, S., Camacho, A., Kucharski, A.J., Lowe, R., Eggo, R.M., and Edmunds, W.J. (2019). Assessing the performance of real-time epidemic forecasts: A case study of Ebola in the Western Area region of Sierra Leone, 2014-15. PLOS Comput. Biol. *15*, e1006785.

Furuse, Y., Ko, Y.K., Saito, M., Shobugawa, Y., Jindai, K., Saito, T., Nishiura, H., Sunagawa, T., and Suzuki, M. (2020). Epidemiology of COVID-19 Outbreak in Japan, January–March 2020. Jpn. J. Infect. Dis. JJID-2020.

Garske, T., Legrand, J., Donnelly, C.A., Ward, H., Cauchemez, S., Fraser, C., Ferguson, N.M., and Ghani, A.C. (2009). Assessing the severity of the novel influenza A/H1N1 pandemic. BMJ *339*.

Ghani, A.C., Donnelly, C.A., Cox, D.R., Griffin, J.T., Fraser, C., Lam, T.H., Ho, L.M., Chan, W.S., Anderson, R.M., Hedley, A.J., et al. (2005). Methods for Estimating the Case Fatality Ratio for a Novel, Emerging Infectious Disease. Am. J. Epidemiol. *162*, 479–486.

Gilbert, M., Dewatripont, M., Muraille, E., Platteau, J.-P., and Goldman, M. (2020). Preparing for a responsible lockdown exit strategy. Nat. Med. 1–2.

Google (2021). COVID-19 Google Community Mobility Reports.

Gostic, K.M., McGough, L., Baskerville, E.B., Abbott, S., Joshi, K., Tedijanto, C., Kahn, R., Niehus, R., Hay, J.A., De Salazar, P.M., et al. (2020). Practical considerations for measuring the effective reproductive number, Rt. PLOS Comput. Biol. *16*, e1008409.

Heesterbeek, J.A.P., and Roberts, M.G. (2007). The type-reproduction number T in models for infectious disease control. Math. Biosci. *206*, 3–10.

Heydari, S.T., Zarei, L., Sadati, A.K., Moradi, N., Akbari, M., Mehralian, G., and Lankarani, K.B. (2021). The effect of risk communication on preventive and protective Behaviours during the COVID-19 outbreak: mediating role of risk perception. BMC Public Health *21*, 54.

Höhle, M. (2007). surveillance: An R package for the monitoring of infectious diseases. Comput. Stat. *22*, 571–582.

Huang, C., Wang, Y., Li, X., Ren, L., Zhao, J., Hu, Y., Zhang, L., Fan, G., Xu, J., and Gu, X. (2020). Clinical features of patients infected with 2019 novel coronavirus in Wuhan, China. Lancet *395*, 497–506.

Imperial College London-MRC Centre for Global Infectious Disease Analysis (2020). Report 3 - Transmissibility of 2019-nCoV.

Jacquez, J.A., and O'Neill, P. (1991). Reproduction numbers and thresholds in stochastic epidemic models I. Homogeneous populations. Math. Biosci. *107*, 161–186.

Japan Meteorological Agency (2021). Climatological data.

Johns Hopkins University (2021). COVID-19 dashboard.

Jung, S., Kinoshita, R., Thompson, R.N., Linton, N.M., Yang, Y., Akhmetzhanov, A.R., and Nishiura, H. (2020a). Epidemiological Identification of A Novel Pathogen in Real Time: Analysis of the Atypical Pneumonia Outbreak in Wuhan, China, 2019–2020. J. Clin. Med. *9*, 637.

Jung, S., Kinoshita, R., Thompson, R.N., Linton, N.M., Yang, Y., Akhmetzhanov, A.R., and Nishiura, H. (2020b). Epidemiological identification of a novel pathogen in real time: Analysis of the atypical pneumonia outbreak in Wuhan, China, 2019–2020. J. Clin. Med. *9*, 637.

Jung, S., Endo, A., Kinoshita, R., and Nishiura, H. (2021). Projecting a second wave of COVID-19 in Japan with variable interventions in high-risk settings. R. Soc. Open Sci. *8*, 202169.

Kishore, N., Kiang, M. V, Engø-Monsen, K., Vembar, N., Schroeder, A., Balsari, S., and Buckee, C.O. (2020). Measuring mobility to monitor travel and physical distancing interventions: a common framework for mobile phone data analysis. Lancet Digit. Heal. *2*, e622–e628.

Kobayashi, T., Jung, S., Linton, N.M., Kinoshita, R., Hayashi, K., Miyama, T., Anzai, A., Yang, Y., Yuan, B., and Akhmetzhanov, A.R. (2020). Communicating the risk of death from novel coronavirus disease (COVID-19). J. Clin. Med. *9*, 580.

Kucharski, A.J., Russell, T.W., Diamond, C., Liu, Y., Edmunds, J., Funk, S., Eggo, R.M., Sun, F., Jit, M., and Munday, J.D. (2020). Early dynamics of transmission and control of COVID-19: a mathematical modelling study. Lancet Infect. Dis. *20*, 553–558.

Lau, H., Khosrawipour, V., Kocbach, P., Mikolajczyk, A., Schubert, J., Bania, J., and Khosrawipour, T. (2020). The positive impact of lockdown in Wuhan on containing the COVID-19 outbreak in China. J. Travel Med. *27*, taaa037.

Leung, K., Wu, J.T., and Leung, G.M. (2021). Real-time tracking and prediction of COVID-19 infection using digital proxies of population mobility and mixing. Nat. Commun. *12*, 1501.

Li, H., Xu, X.-L., Dai, D.-W., Huang, Z.-Y., Ma, Z., and Guan, Y.-J. (2020a). Air pollution and temperature are associated with increased COVID-19 incidence: A time series study. Int. J.

Infect. Dis. *97*, 278–282.

Li, M., Dushoff, J., and Bolker, B.M. (2018). Fitting mechanistic epidemic models to data: A comparison of simple Markov chain Monte Carlo approaches. Stat. Methods Med. Res. *27*, 1956–1967.

Li, Q., Guan, X., Wu, P., Wang, X., Zhou, L., Tong, Y., Ren, R., Leung, K.S.M., Lau, E.H.Y., Wong, J.Y., et al. (2020b). Early Transmission Dynamics in Wuhan, China, of Novel Coronavirus–Infected Pneumonia. N. Engl. J. Med. *382*, 1199–1207.

Linton, N.M., Kobayashi, T., Yang, Y., Hayashi, K., Akhmetzhanov, A.R., Jung, S., Yuan, B., Kinoshita, R., and Nishiura, H. (2020). Incubation Period and Other Epidemiological Characteristics of 2019 Novel Coronavirus Infections with Right Truncation: A Statistical Analysis of Publicly Available Case Data. J. Clin. Med. *9*, 538.

Linton, N.M., Akhmetzhanov, A.R., and Nishiura, H. (2021). Correlation between times to SARS-CoV-2 symptom onset and secondary transmission undermines epidemic control efforts. MedRxiv 2021.08.29.21262512.

Lipsitch, M., Cohen, T., Cooper, B., Robins, J.M., Ma, S., James, L., Gopalakrishna, G., Chew, S.K., Tan, C.C., and Samore, M.H. (2003). Transmission dynamics and control of severe acute respiratory syndrome. Science (80-.). *300*, 1966–1970.

Liu, Y., Eggo, R.M., and Kucharski, A.J. (2020). Secondary attack rate and superspreading events for SARS-CoV-2. Lancet.

Ma, Y., Pei, S., Shaman, J., Dubrow, R., and Chen, K. (2021). Role of meteorological factors in the transmission of SARS-CoV-2 in the United States. Nat. Commun. *12*, 3602.

McClymont, H., and Hu, W. (2021). Weather Variability and COVID-19 Transmission: A Review of Recent Research. Int. J. Environ. Res. Public Health *18*, 396.

Ministry of Health Labour and Welfare (2020a). Basic Policies for Novel Coronavirus Disease Control by the Government of Japan (Summary).

Ministry of Health Labour and Welfare (2020b). Updates on COVID-19 in Japan.

Ministry of Health Labour and Welfare (2020c). Press release.

Ministry of Health Labour and Welfare (2020d). Requests for reducing operation hours from November 2020.

Ministry of Health Labour and Welfare (2020e). Evaluation report for the latest COVID-19 infections.

Ministry of Health Labour and Welfare (2021a). The 50th report from the COVID-19 response advisory board.

Ministry of Health Labour and Welfare (2021b). The 45th report from the COVID-19 response advisory board.

Ministry of Health Labour and Welfare (2021c). The 58th report from the COVID-19 response advisory board.

Ministry of Health Singapore (2020). Tighter Measures to Minimise Further Spread of COVID-19.

Mizumoto, K., Saitoh, M., Chowell, G., Miyamatsu, Y., and Nishiura, H. (2015). Estimating the risk of Middle East respiratory syndrome (MERS) death during the course of the outbreak in the Republic of Korea, 2015. Int. J. Infect. Dis. *39*, 7–9.

National Institute of Infectious Diseases (2020). COVID-19 Situation in Osaka Prefecture.

Nishiura, H., and Chowell, G. (2009). The Effective Reproduction Number as a Prelude to Statistical Estimation of Time-Dependent Epidemic Trends. Math. Stat. Estim. Approaches Epidemiol. 103–121.

Nishiura, H., Klinkenberg, D., Roberts, M., and Heesterbeek, J.A.P. (2009). Early epidemiological assessment of the virulence of emerging infectious diseases: a case study of an influenza pandemic. PLoS One *4*.

Nishiura, H., Jung, S., Linton, N.M., Kinoshita, R., Yang, Y., Hayashi, K., Kobayashi, T., Yuan, B., and Akhmetzhanov, A.R. (2020a). The extent of transmission of novel coronavirus in Wuhan, China, 2020.

Nishiura, H., Kobayashi, T., Miyama, T., Suzuki, A., Jung, S., Hayashi, K., Kinoshita, R., Yang, Y., Yuan, B., and Akhmetzhanov, A.R. (2020b). Estimation of the asymptomatic ratio of novel coronavirus infections (COVID-19). Int. J. Infect. Dis. *94*, 154.

Nishiura, H., Oshitani, H., Kobayashi, T., Saito, T., Sunagawa, T., Matsui, T., Wakita, T., and Suzuki, M. (2020c). Closed environments facilitate secondary transmission of coronavirus disease 2019 (COVID-19). MedRxiv 2020.02.28.20029272.

Nishiura, H., Linton, N.M., and Akhmetzhanov, A.R. (2020d). Serial interval of novel coronavirus (COVID-19) infections. Int. J. Infect. Dis.

Nouvellet, P., Bhatia, S., Cori, A., Ainslie, K.E.C., Baguelin, M., Bhatt, S., Boonyasiri, A., Brazeau, N.F., Cattarino, L., Cooper, L. V, et al. (2021). Reduction in mobility and COVID-19 transmission. Nat. Commun. *12*, 1090.

Osaka Prefectural Gvernment (2020). Emergency information.

Oshitani, H. (2020). Cluster-based approach to coronavirus disease 2019 (COVID-19) response in Japan, from February to April 2020. Jpn. J. Infect. Dis. *73*, 491–493.

Park, S.W., Bolker, B.M., Champredon, D., Earn, D.J.D., Li, M., Weitz, J.S., Grenfell, B.T., and

Dushoff, J. (2020). Reconciling early-outbreak estimates of the basic reproductive number and its uncertainty: framework and applications to the novel coronavirus (SARS-CoV-2) outbreak. J. R. Soc. Interface *17*, 20200144.

Pequeno, P., Mendel, B., Rosa, C., Bosholn, M., Souza, J.L., Baccaro, F., Barbosa, R., and Magnusson, W. (2020). Air transportation, population density and temperature predict the spread of COVID-19 in Brazil. PeerJ *8*, e9322.

Perra, N. (2021). Non-pharmaceutical interventions during the COVID-19 pandemic: A review. Phys. Rep. *913*, 1–52.

Qi, H., Xiao, S., Shi, R., Ward, M.P., Chen, Y., Tu, W., Su, Q., Wang, W., Wang, X., and Zhang, Z. (2020). COVID-19 transmission in Mainland China is associated with temperature and humidity: A time-series analysis. Sci. Total Environ. *728*, 138778.

Read, J.M., Bridgen, J.R.E., Cummings, D.A.T., Ho, A., and Jewell, C.P. (2021). Novel coronavirus 2019-nCoV (COVID-19): early estimation of epidemiological parameters and epidemic size estimates. Philos. Trans. R. Soc. B Biol. Sci. *376*, 20200265.

Riddell, S., Goldie, S., Hill, A., Eagles, D., and Drew, T.W. (2020). The effect of temperature on persistence of SARS-CoV-2 on common surfaces. Virol. J. *17*, 145.

Schneider, C.R., Dryhurst, S., Kerr, J., Freeman, A.L.J., Recchia, G., Spiegelhalter, D., and van der Linden, S. (2021). COVID-19 risk perception: a longitudinal analysis of its predictors and associations with health protective behaviours in the United Kingdom. J. Risk Res. *24*, 294–313.

Shinjyuku City (2021). PCR test in Shinjyuku city.

Smith, T.P., Flaxman, S., Gallinat, A.S., Kinosian, S.P., Stemkovski, M., Unwin, H.J.T., Watson, O.J., Whittaker, C., Cattarino, L., Dorigatti, I., et al. (2021). Temperature and population density influence SARS-CoV-2 transmission in the absence of nonpharmaceutical interventions. Proc. Natl. Acad. Sci. *118*, e2019284118.

Subcommittee on Novel Coronavirus Disease Control (2020). Infection control in night spots.

Subcommittee on Novel Coronavirus Disease Control (2021). 2021 Weekly reports of subcommittee on Novel Coronavirus Disease Control.

The Novel Coronavirus Pneumonia Emergency Response Epidemiology Team (2020). The epidemiological characteristics of an outbreak of 2019 novel coronavirus diseases (COVID-19)—China, 2020. China CDC Wkly. *2*, 113–122.

The RECOVERY Collaborative Group (2020). Dexamethasone in Hospitalized Patients with Covid-19. N. Engl. J. Med. *384*, 693–704.

The University of Hong Kong-HKUMed WHO Collaborating Centre for Infectious Disease Epidemiology and Control Nowcasting and Forecasting the Wuhan COVID-19 Outbreak.

The World Health Organization (2020a). COVID-19 - China.

The World Health Organization (2020b). Novel Coronavirus (COVID-19) Situation Report-3.

Thompson, R.N. (2020). Novel coronavirus outbreak in Wuhan, China, 2020: intense surveillance is vital for preventing sustained transmission in new locations. J. Clin. Med. *9*, 498.

Thompson, R.N., Gilligan, C.A., and Cunniffe, N.J. (2016). Detecting Presymptomatic Infection Is Necessary to Forecast Major Epidemics in the Earliest Stages of Infectious Disease Outbreaks. PLOS Comput. Biol. *12*, e1004836.

Thompson, R.N., Stockwin, J.E., van Gaalen, R.D., Polonsky, J.A., Kamvar, Z.N., Demarsh, P.A., Dahlqwist, E., Li, S., Miguel, E., Jombart, T., et al. (2019a). Improved inference of time-varying reproduction numbers during infectious disease outbreaks. Epidemics *29*, 100356.

Thompson, R.N., Gilligan, C.A., and Cunniffe, N.J. (2019b). When does a minor outbreak become a major epidemic? Linking the risk from invading pathogens to practical definitions of a major epidemic. BioRxiv 768853.

Tokyo Metropolitan Government (2020a). Latest information.

Tokyo Metropolitan Government (2020b). Press conference.

Tokyo Metropolitan Government (2020c). Press conferecne.

Ujiie, M., Tsuzuki, S., and Ohmagari, N. (2020). Effect of temperature on the infectivity of COVID-19. Int. J. Infect. Dis. *95*, 301–303.

Wallinga, J., and Lipsitch, M. (2007). How generation intervals shape the relationship between growth rates and reproductive numbers. Proc. R. Soc. B Biol. Sci. *274*, 599–604.

Wang, J., Tang, K., Feng, K., Lin, X., Lv, W., Chen, K., and Wang, F. (2021). Impact of temperature and relative humidity on the transmission of COVID-19: a modelling study in China and the United States. BMJ Open *11*, e043863.

West, R., Michie, S., Rubin, G.J., and Amlôt, R. (2020). Applying principles of behaviour change to reduce SARS-CoV-2 transmission. Nat. Hum. Behav. *4*, 451–459.

Xiong, C., Hu, S., Yang, M., Luo, W., and Zhang, L. (2020). Mobile device data reveal the dynamics in a positive relationship between human mobility and COVID-19 infections. Proc. Natl. Acad. Sci. *117*, 27087 LP – 27089.

Zhao, S., Lin, Q., Ran, J., Musa, S.S., Yang, G., Wang, W., Lou, Y., Gao, D., Yang, L., and He, D. (2020). Preliminary estimation of the basic reproduction number of novel coronavirus (2019-nCoV) in China, from 2019 to 2020: A data-driven analysis in the early phase of the outbreak. Int. J. Infect. Dis. *92*, 214–217.